Novel Orange-Emitting $YPO_4:Sm^{3+}$/Polymer Nanocomposite Phosphor Films for LED Applications

Lamine Mebarki [a], Badis Kahouadji [b *], Abdelhalim Zoukel [f,g], Lyes Benharrat [c], Jai Prakash [d,e], Salim Ouhenia [a], Abdelhafid Souici [a], Maxime Delaey [L], Lakhdar Guerbous [k], Dirk Poelman [L], Hendrik C Swart[e]

[a] Laboratory of Physical-chemistry, University of Bejaia, Bejaia, 06000, Algeria.
[b] Department of Technology (El Kseur Campus), Laboratory of Physical-chemistry, University of Bejaia, Bejaia, 06000, Algeria.
[c] Research Center in Semiconductors Technology for Energy-CRTSE, 02, Bd. Dr. Frantz Fanon, B.P. 140,7 Merveilles, 16038, Algiers, Algeria.
[d] Department of Chemistry, National Institute of Technology Hamirpur, Hamirpur (H.P.)-177005, India.
[e] Department of Physics, University of the Free State, Bloemfontein, ZA9300, South Africa.
[f] Technical Platform of Physico-Chemical Analysis (PTAPC-Laghouat-CRAPC), Laghouat, Algeria.
[g] Laboratory Physico-Chemistry of Materials, Laghouat University, Technical Platform of Physico-Chemical Analysis (PTAPC-Laghouat-CRAPC), Laghouat, Algeria.
[h] Department of TCSN, University of Bejaia, Bejaia, 06000, Algeria
[k] Laser Department/ Nuclear Research Centre of Algiers (CRNA), 02, Boulevard Frantz Fanon, B.P. 399, Algiers, 16000, Algeria
[L] Department of Solid State Sciences, Ghent University, Krijgslaan 281-S1 B-9000, Ghent, Belgium.

***Corresponding author**: badis.kahouadji@univ-bejaia.dz

Abstract

A polymer based nanocomposite (NC) material embedded with highly luminescent nanopowders could be promising for replacing traditional luminescent materials from a technological point of view. In this study, we have successfully obtained YPO_4: Sm^{3+} /Polymer nanocomposite phosphor films by embedding YPO_4: Sm^{3+} luminescent nanoparticles (NPs) for orange-light emitting diode (LED) applications. These luminescent NPs were synthesized using the sol gel method in different polymer matrices i.e. polystyrene (PS) and poly (methyl methacrylate) (PMMA) by using direct solution mixing. The structural, morphological, and photoluminescence characteristics of the nano-phosphors and resulting NC films were examined and discussed. The emission spectra of YPO_4: Sm^{3+} (x at.%) nano-phosphors under near-UV excitation at 404 nm were dominated by orange emission attributed to $^6H_{5/2} \rightarrow {}^4F_{7/2}$ (601 nm) luminescence of Sm^{3+} ions. The optimum doping concentration of activator Sm^{3+} in YPO_4 matrix was found to be 5 at.%. When the doping concentration of Sm^{3+} was higher than 5 at.%, concentration quenching occurred. The incorporation of YPO_4: Sm^{3+} NPs into polymer matrices indicated that the NCs retained the original luminescence properties of the luminescent NPs, although a decrease in their emission intensity was observed for the NC films, attributable to a polymer matrix effect, which dominated in PS

matrix. The fluorescence decay times of NPs in the NC films were measured and compared to those of proper YPO_4: Sm^{3+} nano-phosphors. A decrease in decay time in NC film was observed due the effective refractive index effect. Temperature-dependent photoluminescence (TDPL) of PMMA NC film was studied in 100-400 K range, investigating the thermal stability of the film. Additionally, CIE coordinates confirmed the red-orange light emission of the prepared phosphors and NC films. The obtained results indicate that the synthesized polymer-nanophosphor NC films are promising candidates for orange-LED applications.

Keywords : YPO_4:Sm^{3+} NPs ; Nanophosphors, Luminescent NC films ; Photoluminescence; LED applications.

1. Introduction

Solid-state semiconductor lighting technology began its development in the 1960s with the advent of the first semiconductor diode lasers. Initially, their use was restricted to applications such as digital displays or light indicators due to their longer wavelengths [1]. However, in 1993, Shuji Nakamura's major innovation changed the game with the creation of the first efficient blue LED devices, thus paving the way for broader commercial applications [2]. Since then, significant progress has been made, notably with the production of the first white LED in 1996 [4]. This development has spawned an extensive industrial chain, encompassing the growth of epitaxial films, preparation of white LEDs and packaging materials along with diverse range of applications such as digital displays, household lighting etc. [5], [3].

Over the past decade, significant advancements have been made in the design and development of optoelectronic systems largely attributable to innovations in light sources. However, there remains significant potential for the development of compact, efficient, and cost-effective light sources in the visible spectrum [6]. The composite materials based on polymers loaded with highly luminescent nanopowders could present a promising approach to effectively replace traditional luminescent materials. Nanocomposites (NCs) are a specific category of composite materials where nano- or molecular-sized particles are incorporated into organic polymers, metals, or ceramics [7]. This close inclusion of nanoparticles (NPs) in matrices can significantly alter the mechanical, electrical, and optical properties of these materials [8]. Currently, the demand and market for polymers are experiencing sustained growth, primarily due to their affordable cost and attractive physical, mechanical, and chemical properties [9-10]. These materials offer advantages such as ease of molding,

strength, and inertness, which are generating great interest in industry [10]. Consequently, numerous theoretical and experimental efforts are focused on developing new strategies to optimize the properties of hybrid systems, such as polymers incorporating nanoscale inorganic materials. To enhance the properties of this class of materials, obtaining precise NPs morphology and size in the polymer matrix are essential [12]. However, controlling their spatial arrangement is challenging due to the immiscibility of inorganic particles, leading to the formation of large aggregates in polymer nanocomposites (PNCs) [11-12]. Such an outcome could have a degrading effect on the optical properties of the NCs, as it has been demonstrated that large aggregates cause light scattering, reducing the material's transmittance [13]. To address this issue, many approaches are explored in the literature, among which self-assembly stands out as a particularly powerful method for the fabrication of functional materials [12-14]. This approach involves manipulating the morphology of NP by adjusting their interactions at the molecular level. In other words, this process proposes modifying the surface properties of NPs by combining them with different types of ligands, such as small molecules and copolymers [15]. Despite its promising potential for controlling the distribution of NPs by adjusting their interaction modes, self-assembly faces significant challenges when it comes to large-scale implementation. This difficulty likely arises from the complexity of the organization and assembly processes of aggregates, particularly when NPs exhibit anisotropic morphology [12-16]. Specifically, the preparation of high-performance polymer/filler nanocomposites, by co-dissolving NPs and the polymer matrix in the same solvent, followed by rapid precipitation and drying, improves dispersibility [18]. Studies show that the complex interactions between polymer, NPs, and solvent affect the dispersion of NPs in solution. Experimental results sometimes diverge from theoretical models, highlighting the importance of considering all interactions in the system. Where the balance of interactions between the constituents is encoded at the level of a few parameters such as the size and concentration of NPs, the kinetics of solvent removal and dilution further unifies the structures of mixed PNCs in solution [17]. In this context, several scientific works have been carried out. For example, Khursheed et al. reported a successful synthesis of PNCs films of $KCaVO_4$:Sm^{3+}(1.5 mol%)/Polymethyl methacrylate (PMMA), using the solution casting method. The results showed characteristic luminescent emissions of Sm^{3+} ions in the orange-red color range, as well as an increase in thermal stability and glass transition temperature compared to pure polymer [19]. As another example, nano-phosphors Gd_2O_3: Er^{3+} with a size of about 12 nm were mixed with polymers in PMMA and polycarbonate (PC) solution forming PNCs with excellent optical properties. The characterization results confirmed that

nanocomposite films doped with Gd_2O_3: Er^{3+} exhibited high color stability and appreciable color tunability from yellow to red-orange was achieved. Therefore, these new classes of PNCs can be used in various lighting and photonic applications [20]. Similarly, research conducted by Dudek et al. aimed to study the luminescent properties of such PNCs in different parts of the visible spectrum (blue, green, and red) and understand how Y_2O_3:Pr^{3+} and $LaAlO_3$:Pr^{3+} NPs reacted when incorporated into a polymer matrix [21]. The ultimate goal is to demonstrate that these PNCs can effectively retain the optical properties of active NPs and offer potential for the design of new optically active polymer components, particularly for low-cost light sources.

Yttrium orthophosphate (YPO_4) has been recognized as an ideal structure to host rare earth activator ions. This has sparked research interest due to its numerous advantages: remarkable chemical and optical properties, reduced toxicity, and good resistance to photochemical degradation [24]. By doping this host material with trivalent samarium (Sm^{3+}), intense red-orange light emission in the visible range is obtained under UV excitation. This fluorescence arises from the electronic transition $^6H_{5/2} \rightarrow {}^4F_{7/2}$ of Sm^{3+}. Thus, the idea of incorporating these nano-phosphors into transparent matrices such as polymers is attractive for the development of new cost-effective light sources suitable for a wide range of applications, including solid state lighting, display devices, high-definition televisions, field emission displays, latent fingerprint detection, medical sciences, etc. [22], [23]. However, before achieving this goal, it is crucial to study the behavior of YPO_4:Sm^{3+} NPs in different polymers (ensuring good compatibility) and to understand the excitation energy transfer from the luminescence centers of NPs within the polymer matrix.

The present study demonstrates a successful synthesis of flexible luminescent PNCs films, marking the first-time YPO_4 NPs doped with samarium (YPO_4: Sm^{3+}) incorporated into PMMA and polystyrene (PS) matrix through a direct mixing process in solution followed by shaping into thin films. The obtained films were studied and analyzed using spectroscopic and microscopic techniques. The structural, morphological, and photoluminescence properties of the films were examined for their potential application in lighting.

2. Experimental

2.1. YPO_4: Sm^{3+} nanopowders synthesis

Nanophosphors of samarium-doped yttrium orthophosphate (YPO_4:Sm^{3+}) were synthesized in powder form using an experimental protocol based on the sol-gel method. A series of YPO_4: xSm^{3+} (x =1, 3, 5, 8, 10 at.%) nanopowders were synthesized in similar experimental conditions.

Initially, a stoichiometric proportion of Y_2O_3 (99.99% Sigma-Aldrich), Sm_2O_3 (99.99% Sigma-Aldrich), and $(NH_4)_2HPO_4$ (>99.0%) precursors was dissolved in a suitable solvent (deionized water + nitric acid, 100 ml: 5 ml). The resulting mixture was stirred for 12 hours to dissociate the precursors, forming a homogeneous transparent solution. Then, a quantity of organic agents (ethylene glycol, EG) was added and stirred for 2 hours. Subsequently, the pH of the solution was adjusted to a value of 2 (acidic medium) by adding NH_4OH. Finally, the resulting solution was dried at 150 °C and annealed at 900 °C for 4 hours, thus a white powder compound of YPO_4:Sm^{3+} was obtained. The different steps of this experimental protocol have been detailed in our previous work [25].

2.2. Synthesis of YPO_4: Sm^{3+}/Polymer NC films

Thin nanocomposite films NCs of YPO_4: Sm^{3+}/polymer were prepared by incorporation of YPO_4: Sm^{3+} NPs in two polymers matrix PMMA and PS using the direct solution mixing method.

In this experimental protocol, 1 g of polymer crystals (granules) was dissolved in an amount of chloroform ($CHCl_3$). The (polymer/chloroform) mixture was magnetically stirred until complete dissolution of the polymer for the formation of a homogeneous viscous solution. Subsequently, a quantity of YPO_4: Sm^{3+} nanopowder, with a mass ratio $\frac{\mathrm{m}\,(YPO_4:\mathrm{Sm}^{3+})}{\mathrm{m}\,(\mathrm{Polymer})} = 10\%$, was added to the obtained solution, followed by extended agitation for 12 hours to ensure the uniform dispersion of YPO_4: Sm^{3+} nanoparticles in the solution. Finally, the YPO_4: Sm^{3+} / Polymer solution was spread onto a glass substrate and dried at room temperature for 24 hours, thus a nanocomposite film with an approximate thickness of 100 μm was obtained. Fig. 1 illustrates the different stages of the PNC films synthesis process.

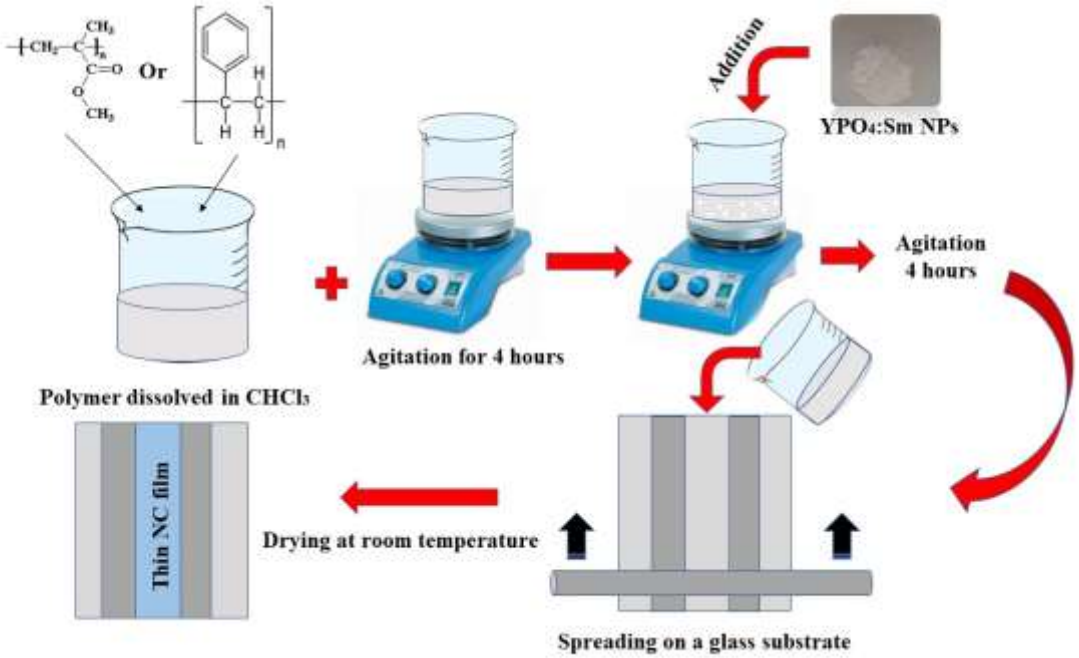

Fig. 1 Synthesis steps of the YPO_4: Sm^{3+}/PNC films

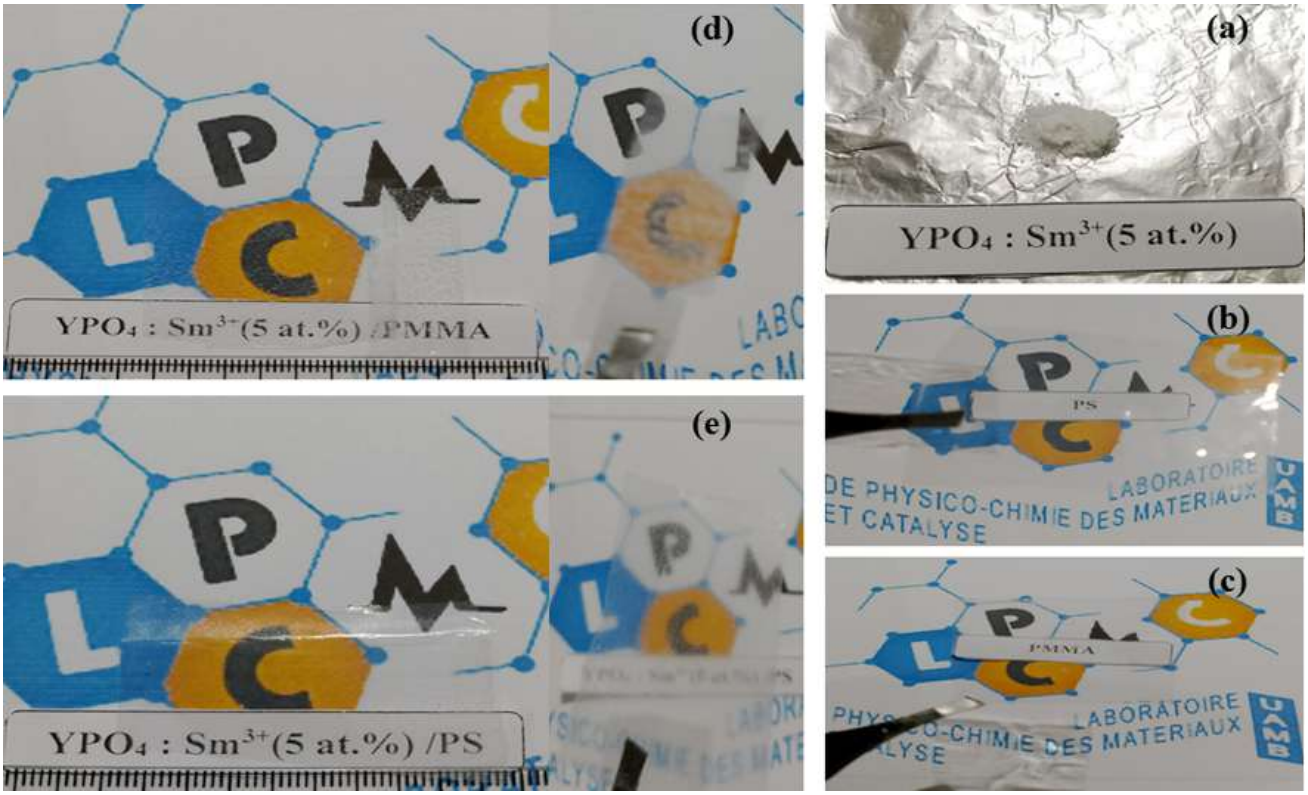

Fig. 2 Photograph of the prepared nanophosphor and films (a) YPO_4: Sm^{3+} (5 at. %) nanopowder, (b) Pure PS, (c) Pure PMMA, (d) YPO_4: Sm^{3+} (5 at. %) /PMMA, (e) YPO_4: Sm^{3+} (5 at. %) /PS

2.3 Characterization techniques

The crystalline structure of the YPO_4: Sm^{3+} nanopowders, as well as the NPCs films, were studied by using the X-ray diffraction (XRD) technique using a Rigaku Mini flex-II diffractometer using CuK_α radiation (λ =1.54059 Å) operated at 30 kV and 15 mA exploring the 2θ angular range 10-80° with a scan step of 0.02° (2θ). The average crystallite sizes and the microstructure were refined using the Rietveld method with the MAUD software for the YPO_4 phase based on the JCPDS data card N° 011-0254. Surface morphology and microstructure of the samples were investigated using a Quattro ESEM scanning electron microscope (SEM) and a Talos™ F200X G2 transmission electron microscope (TEM).

Fourier transform infrared (FT-IR) spectra were recorded using a Perkin Elmer "spectrum two", over a range of 400 to 4000 cm^{-1} with an optimal resolution of 0.5 cm^{-1}. Photoluminescence measurements were performed using a FL3-DFX-iHR luminescence spectrometer (Horiba, Jobin Yvon) equipped with continuous and pulsed xenon lamps, and Edinburgh Instruments - FLS1000-DD-stm for temperature-dependent photoluminescence measurements.

3. Results and discussion

3.1 Structural and morphological characterization

3.1.1. XRD analysis

The XRD patterns of YPO_4: xSm^{3+} (x = 1, 3, 5, 8, 10 at.%) nanopowders annealed at 900 °C for 4 hours are presented in Fig. 3. The X-ray diffractograms indicate that all observed diffraction peaks correspond to the pure tetragonal phase of the YPO_4 matrix (xenotime structure, space group $I4_1/amd$) according to JCPDS data files N° 011-0254.

The introduction of Sm^{3+} ions as a dopant into the YPO_4 matrix does not alter the nature of the obtained phase. However, the partial substitution of Y^{3+} ions by Sm^{3+} ions slightly modifies the lattice parameters. The evolution of the lattice volume, as a function of the concentration of Sm^{3+} ions, and the various crystallographic and microstructural parameters of YPO_4: Sm^{3+} (x at.%) nanopowders, obtained using the MAUD software after refining the recorded XRD patterns, are summarized in Table 1. A slight increase in the lattice volume is observed with the growth of the doping level, attributed to the larger ionic radius of Sm^{3+} ions (0.96A°) [26] as compared to that of Y^{3+} ions (0.90 A°) [27], resulting in lattice expansion during substitution. This aligns with the result obtained by other authors [30].

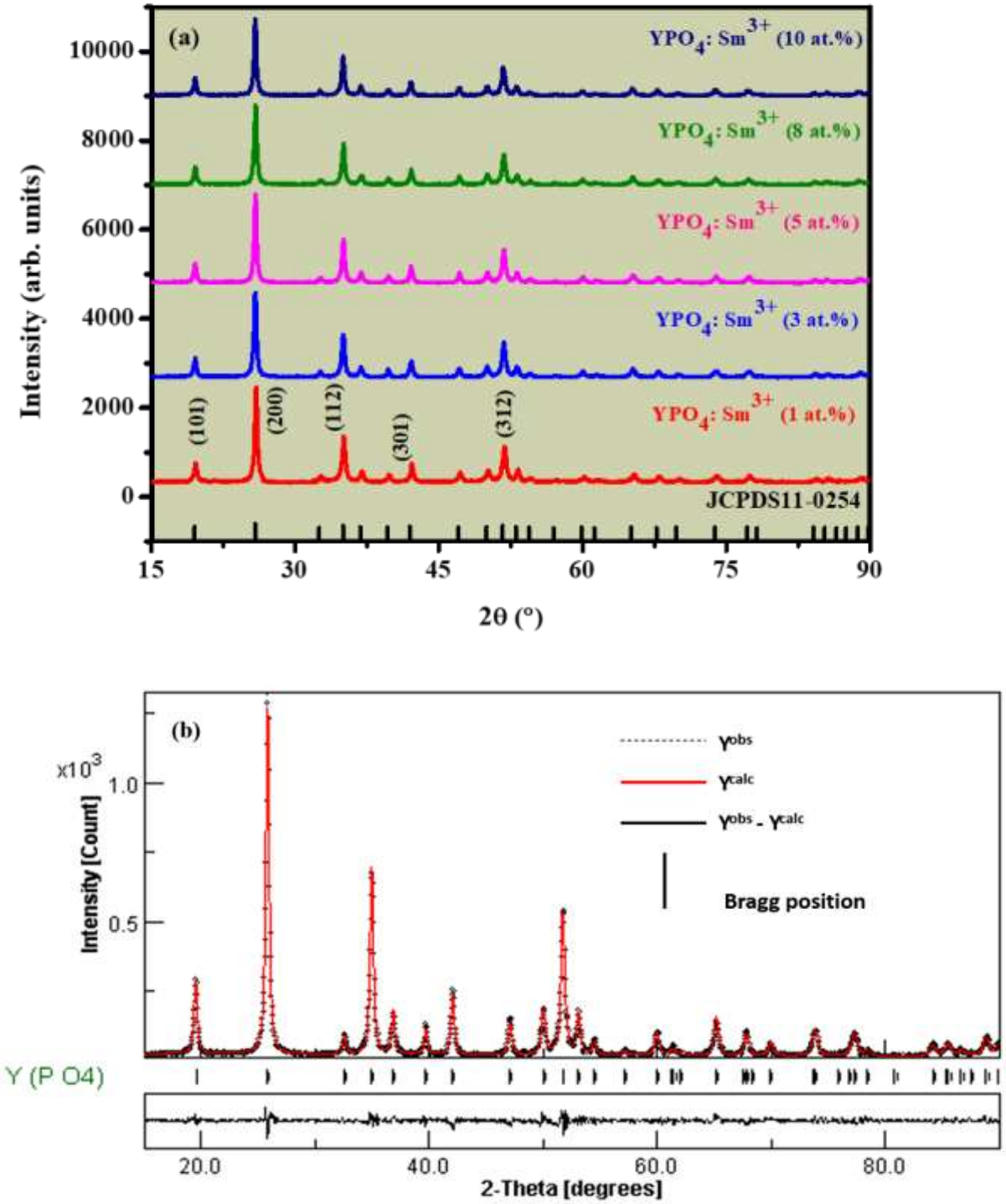

Fig.3 (a) XRD patterns of the YPO_4: Sm^{3+} (x at. %) nanopowders, (b) Calculated (lines), observed (dots), and difference curves after the last cycle of Rietveld refinement

Table.1 Crystallographic parameters of $YPO_4:Sm^{3+}$ (x at. %) nanopowders using MAUD software

Concentration (x at.% Sm^{3+})	Crystallite size (A°)	Lattice volume (A^3)	a (A°)	c (A°)	GoF
1	391(3)	286.60	6.8949(2)	6.0301(3)	1.023
3	402(1)	287.02	6.8983(3)	6.0317(4)	0.902
5	427(2)	287.20	6.9001(4)	6.0322(4)	0.940
8	411(3)	287.82	6.9045(4)	6.0375(5)	0.966
10	438(4)	288.18	6.9076(4)	6.0397(5)	0.924

GoF: goodness of fit

Fig.4 shows the XRD analysis of PNCs films with different polymer matrices i.e. PS and PMMA. The X-ray diffractograms of YPO_4: Sm^{3+}(5 at. %)/PMMA NC and pure PMMA films are shown in Fig. 4 (a). Two diffraction bands are observed at 2θ=16° and 2θ=31°, attributed to the amorphous phase of the PMMA polymer matrix [28], [29]. The XRD diffractogram of PMMA NC film presents several diffraction peaks observed at 2θ = 19.56°, 26°, 35.11°, 42.11°, and 51.77°, which are indexed to the (101), (200), (112), (301), and (312) diffraction planes respectively, attributed to the crystalline structure of YPO_4 xenotime phase according to the JCPDS File No. 011-0254. Fig.4(b) illustrates the XRD patterns of YPO_4: Sm^{3+}(5 at.%)/PS NC film compared to a pure PS film. The result reveals the appearance of a broad band located at 2θ=20°, attributed to the amorphous phase of pure PS matrix [31]. Additionally, diffraction peaks attributed to YPO_4 phase were observed in XRD diffraction patterns of PS NC film. No additional peaks or shifts were observed in the PNC films, however, a decrease in diffraction intensity is noticeable for PS based PNC film compared to PMMA based PNC film that can be explained by calculating the crystallinity degree of the films using the following formula [32].

$$Xc(\%) = \frac{\boldsymbol{Ac}(area\ of\ all\ crystalline\ peaks)}{\mathbf{A_t}\ (\text{area of total peaks})}\ X\ 100 \qquad (1)$$

The calculated crystallinity degree is presented in Table.2.

Table. 2 The calculated crystallinity from XRD patterns NC films

Film	Crystalline area	Total area	Crystallinity Xc (%)
YPO_4: Sm^{3+}/PS	382	2011	19
YPO_4: Sm^{3+}/PMMA	1055	3406	31

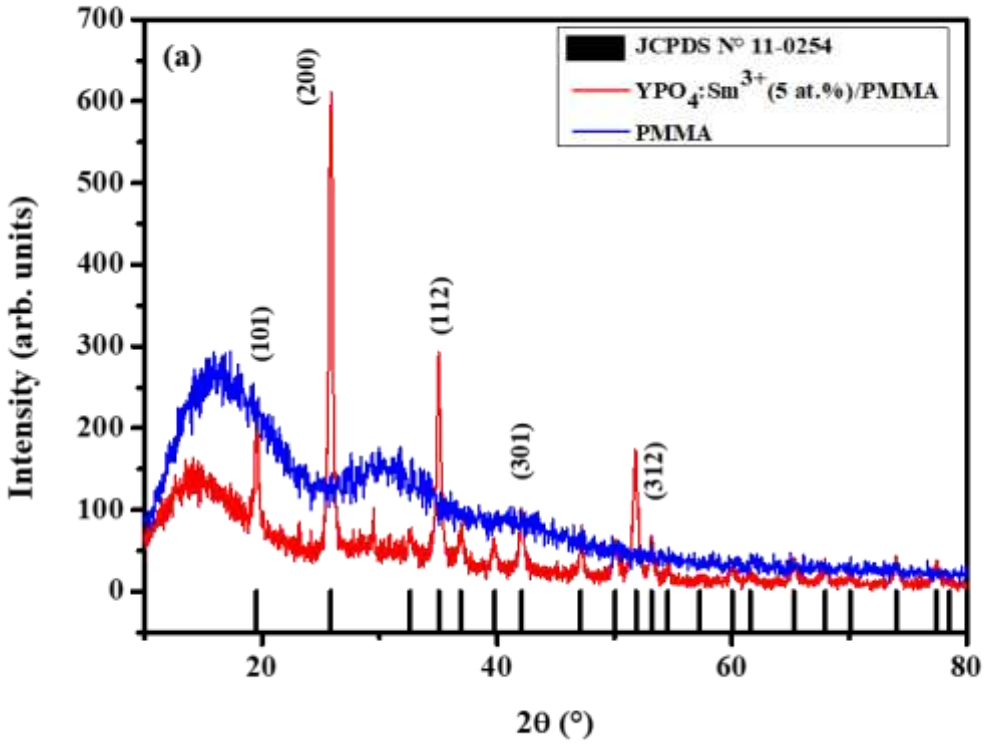

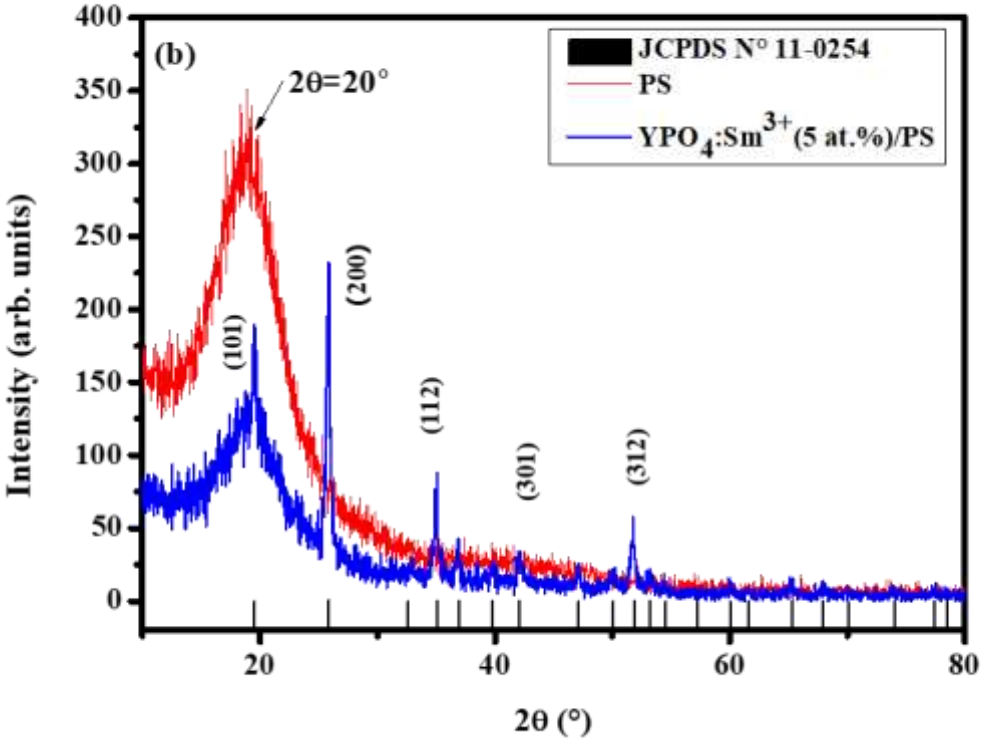

Fig.4 XRD patterns of NCs Film, (a) YPO_4: Sm^{3+} (5 at. %) /PMMA and Pure PMMA film, (b) YPO_4: Sm^{3+} (5 at. %) /PS and pure PS film.

3.1.2 FT-IR spectroscopy

In order to identify the different chemical elements and functional groups present in the prepared samples, FT-IR spectra were recorded in the range of 4000 to 400 cm^{-1}.

Fig. 5(a) shows FT-IR spectrum of YPO_4: Sm^{3+} (5 at.%) nanopowder calcined at 900 °C for 4 hours. Three absorption bands are observed, an intense absorption band, ranging from 1170 to 910 cm^{-1}, corresponding to the antisymmetric stretching vibration of the $(PO_4)^{-3}$ groups [33,34], two other absorption bands located at 646 and 523 cm^{-1} attributed to the deformation of the O-P-O and Y-O or Sm-O bonds respectively [35, 36]. The analysis and results obtained did not reveal any residual chemical elements related to the synthesis process (solvent). This means that all chemical residues present in the powder were eliminated after undergoing thermal treatment at 900 °C.

The FT-IR analysis results of the YPO_4: Sm^{3+} (5 at.%)/PMMA PNC and pure PMMA films are presented in Fig. 5(b). Several characteristic absorptions bands of PMMA are observed at

3000-700 cm^{-1}range, the absorption band at 2810-3000 cm^{-1} range corresponds to the stretching vibrations of the C-H bond, emanating from both the methyl group of the acetone function and the pendant methyl groups of the main chain [38]. A decrease in transmittance is observed in this region in the case of PMMA based PNC films i.e. YPO_4: Sm^{3+} (5 at. %)/PMMA. Additionally, a notable absorption band at 1722 cm^{-1} is observed, resulting from the stretching vibrations of the C=O bond of the acetone function [39,40]. Others characteristic absorption bands at 1444 cm^{-1} and 1238 cm^{-1} are attributed to various modes of deformation of the C-H bond of the methyl part and stretching vibrations of C-C-O respectively [37]. Two absorption bands are also observed at 1195 – 749 cm^{-1} range, corresponding to C-O-C and vibrations respectively [41]. In the region below 700 cm^{-1}, only in the spectrum of the NC/PMMA film, two absorption bands at 640 and 523 cm^{-1} are observed, corresponding to the YPO_4 matrix witch are attributed respectively to the O-P-O and Y-O deformation modes.

Fig. 5(c) shows the FT-IR spectrum of PS based PNC i.e. YPO_4: Sm^{3+} (5 at. %)/PS and PS films. In the PS film, an absorption band at 3110 -2800 cm^{-1} range is observed, resulting from the stretching vibrations of C-H in the main chain and phenyl aromatic units [42]. Absorption bands appearing at 1600, 1490, and 1450 cm^{-1} are attributed to C=C bond vibrations [43,44]. The last three bands identified at 756, 698, and 550 cm^{-1} are assigned to C-H group vibrations [45]. The FT-IR spectra of the YPO_4: Sm^{3+}/PS film exhibit a similar profile to the PS film spectrum. However, new absorption bands localized at 1000 and 640 cm^{-1} are observed in the FT-IR spectra of the PS based PNC film, attributed to the $(PO_4)^{3-}$ and Y-O vibration groups respectively [46-47]. Ultimately, it can be concluded that the absorption bands of the two polymer matrices, namely PMMA and PS, were not affected by the encapsulated YPO_4 NPs. This attests to the presence of nano-phosphors at the core of the developed PNC. The results are consistent with the XRD analysis and suggest that the NPs were formed in pure phase and no parasitic phase was detected in the PNC film. These properties make them suitable for use as PNC phosphor films in LED applications.

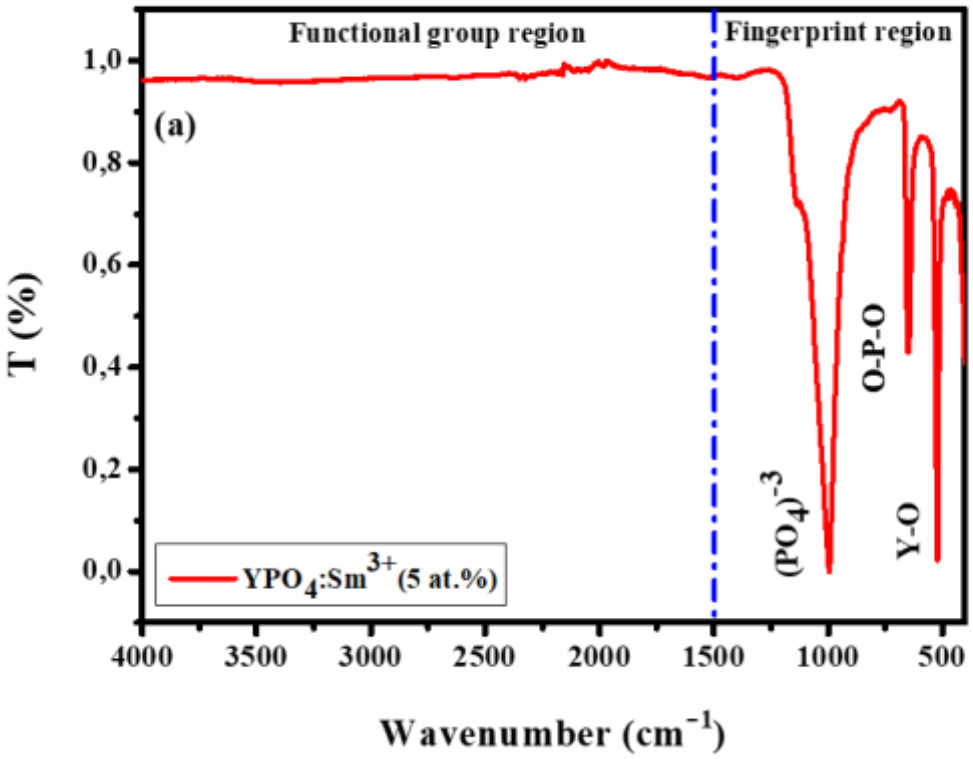
Functional group region
Fingerprint region
(a)
T (%)
1,0
0,8
0,6
0,4
0,2
0,0
4000
3500
3000
2500
2000
1500
1000
500
Wavenumber (cm^{-1})
YPO$_4$:Sm^{3+}(5 at.%)
(PO$_4$)$^{-3}$
O-P-O
Y-O

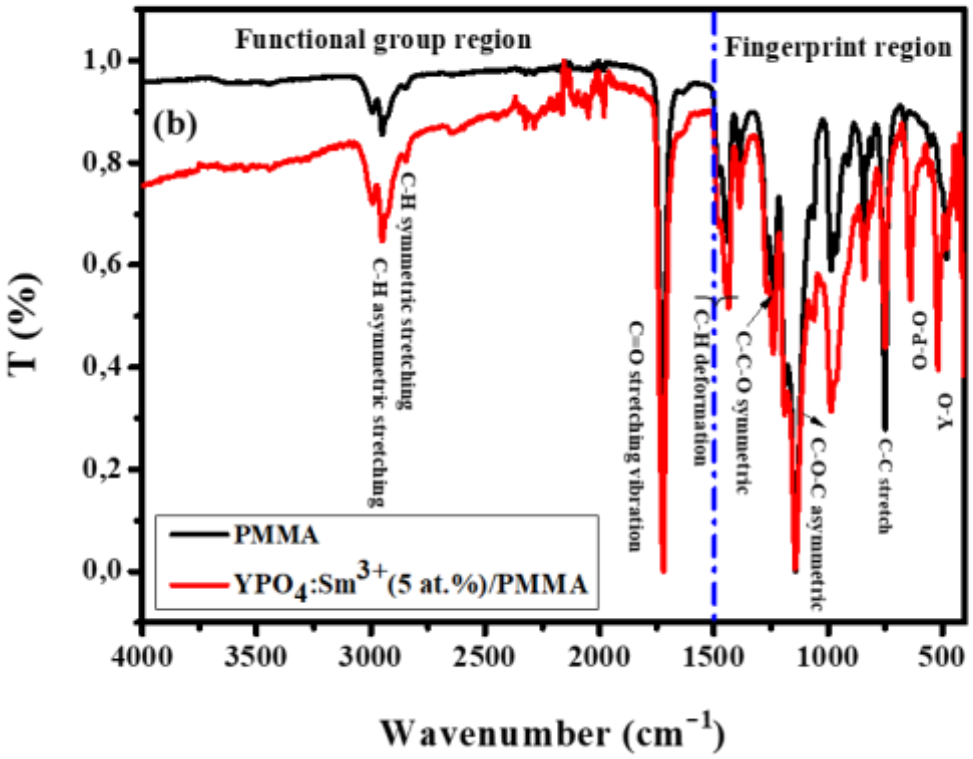
Functional group region
Fingerprint region
(b)
C-H symmetric stretching
C-H asymmetric stretching
C=O stretching vibration
C-H deformation
C-C-O symmetric
C-O-C asymmetric
C-C stretch
O-P-O
Y-O
PMMA
YPO4:Sm3+(5 at.%)/PMMA
T (%)
Wavenumber (cm-1)

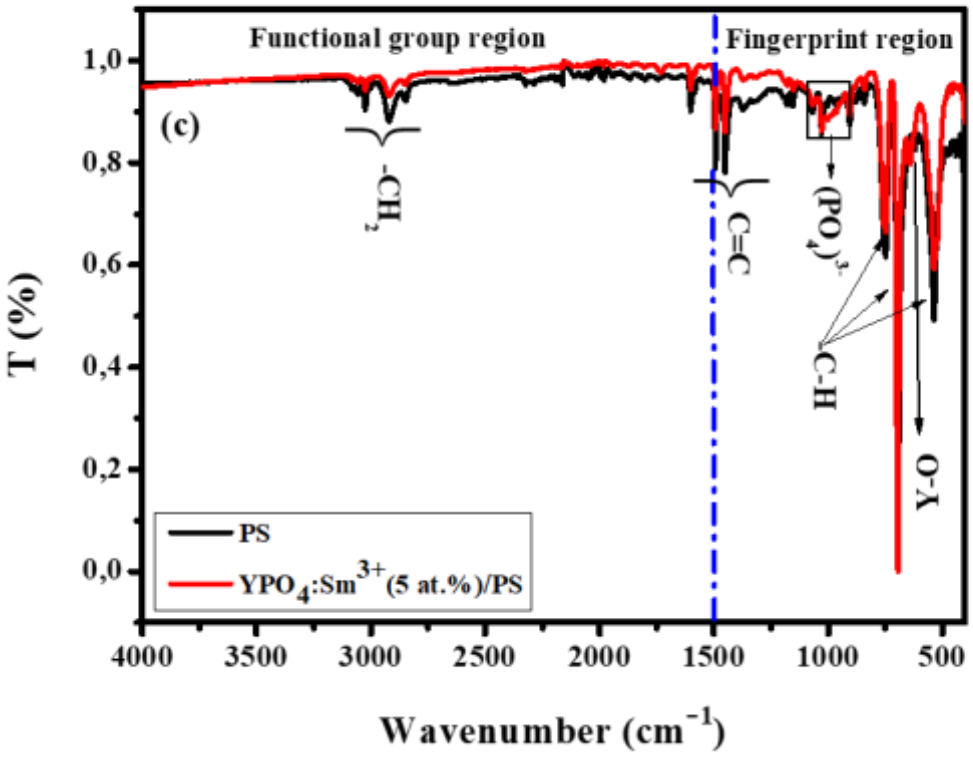
Functional group region
Fingerprint region
(c)
-CH2
C=C
(PO4)3-
C-H
Y-O
PS
YPO4:Sm3+(5 at.%)/PS
T (%)
Wavenumber (cm-1)

Fig. 5 FT-IR spectra of (a) the $YPO_4:Sm^{3+}$ (5 at. %) nanopowder annealed at 900 °C, (b) the $YPO_4:Sm^{3+}$/ PMMA PNC and pure PMMA films, (c) the $YPO_4:Sm^{3+}$/ PS PNC and pure PS films.

3.1.3. Morphological analysis

Fig.6 shows the SEM micrograph of $YPO_4:Sm^{3+}$(5 at.%) NPs which confirms the presence of $YPO_4:Sm^{3+}$ NPs with quasi spherical shapes with an average size of less than 50 nm.

The SEM micrographs of pure PS and PMMA films are shown in Fig. 7(a-b) respectively. These SEM images present flat and featureless and rather clean surfaces, however, embedding the $YPO_4:Sm^{3+}$ nano-phosphors within polymer the matrix led to the alteration of polymer's surface. Fig. 7(c) shows the surface microscopy of the PMMA based PNC films i.e. $YPO_4:Sm^{3+}$/PMMA film, incorporating 10 wt.% of NPs. The analysis of this image highlights the presence of dispersed aggregates, with an average size of approximately 350 nm, uniformly distributed on the surface of the PMMA polymer. The morphology of YPO_4: Sm^{3+}/PS NC (see Fig. 7(d)) generally exhibits a surface with relief textures. This could result from the agglomeration of $YPO_4:Sm^{3+}$ NPs near the surface, attributed to their interconnection with primary NPs. Similar morphological configurations have been reported in PNC films incorporating $ZnO:Tb^{3+}$ phosphors [48]. Prakash et al. noted that phosphor NPs were well dispersed in the polymer film, although some had agglomerated, forming protruding aggregates of primary NPs on the surface of the NC film [49].

3.1.4. EDX analysis

The atomic and weight proportions of the elements in the PNC films of YPO_4: Sm^{3+}(5% at) / polymer have been depicted in the Fig. 8 using EDX analysis. The results of this analysis reveals distinct peaks attributed to the following elements: carbon (C) and oxygen (O), with elevated proportions associated with the organic matrix. Additionally, other chemical signatures are also confirmed, such as the presence of elements such as phosphorus (P), yttrium (Y), and samarium (Sm), suggesting the incorporation of YPO_4 NPs into the polymer film. When excluding the high carbon concentration (from the polymer) from the EDX analysis, it is seen that the ratio's of Y, P, O and Sm properly match the intended stoichiometry within the limits of accuracy of the EDX method.

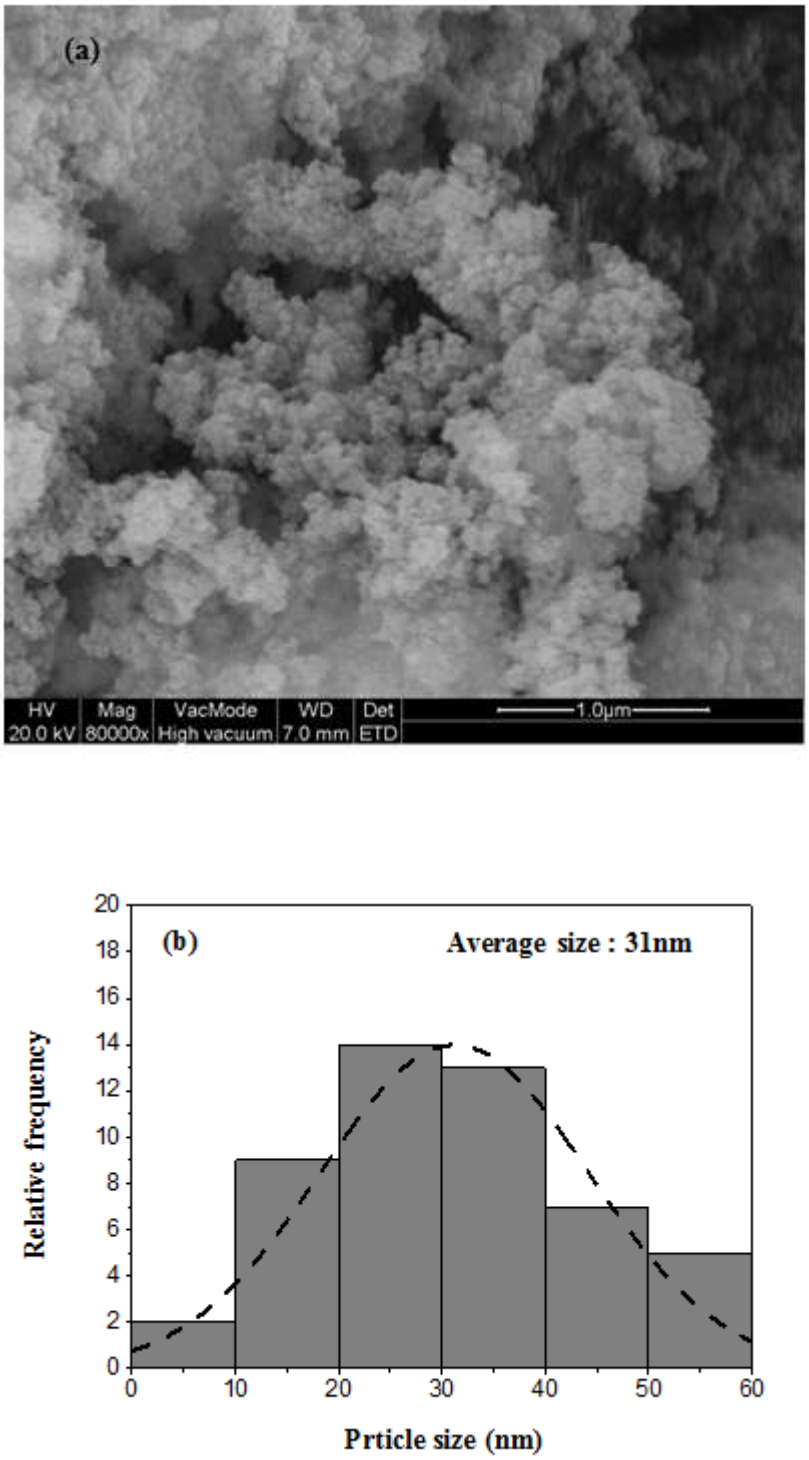

Fig.6 (a) SEM image of $YPO_4:Sm^{3+}$ (5at.%) NPs , (b) particle size distribution histogram

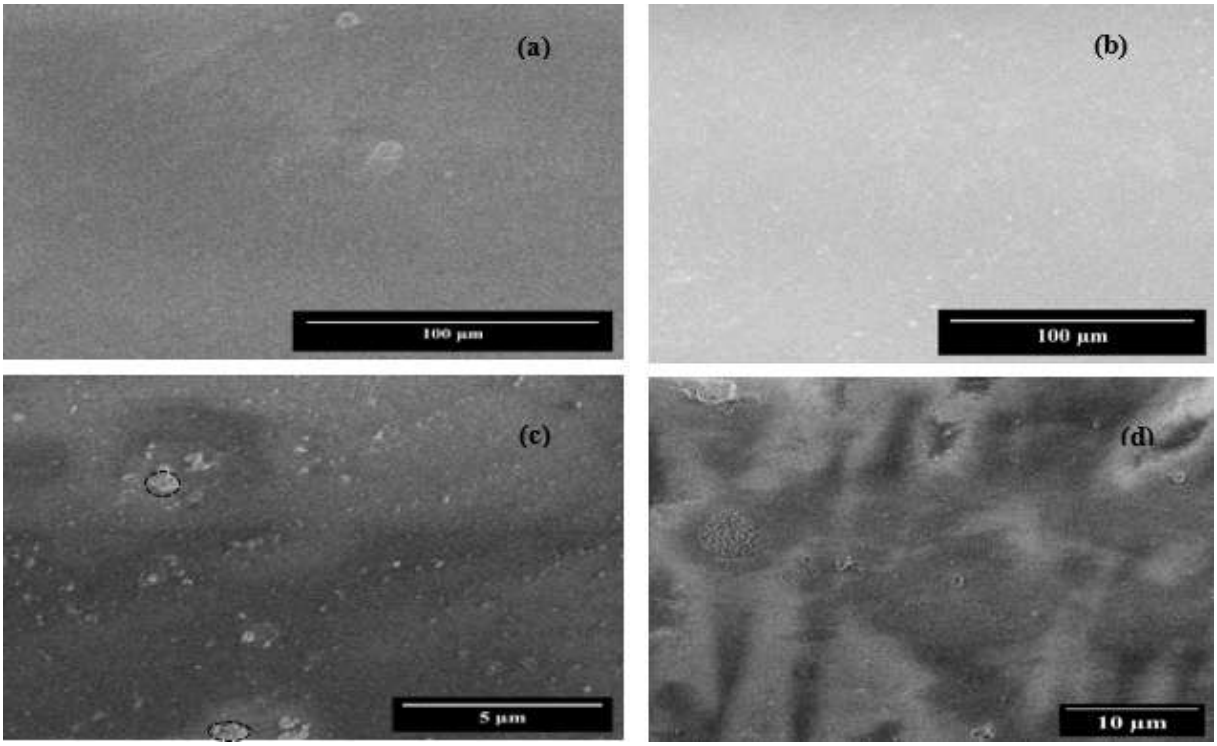

Fig.7 SEM micrographs of pure (a) PS film and (b) PMMA film with corresponding PNC films (c) $YPO_4:Sm^{3+}$/PMMA PNC and (d) $YPO_4:Sm^{3+}$/PS PNC films

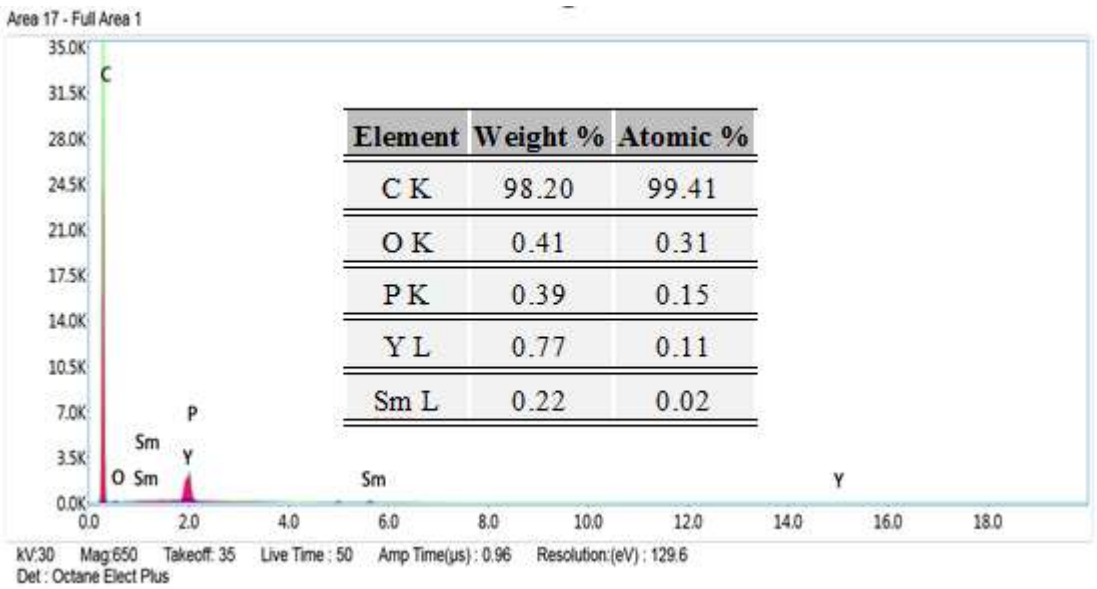

Element	Weight %	Atomic %
C K	98.20	99.41
O K	0.41	0.31
P K	0.39	0.15
Y L	0.77	0.11
Sm L	0.22	0.02

Fig.8 EDX analysis of YPO_4: Sm^{3+}(5 at.%)/PS PNC film.

3.2. UV-Visible spectroscopy

An in-depth investigation of the optical properties of synthesized films was conducted using UV-Vis spectroscopy in absorbance mode, covering the wavelength range from 200 nm to 800 nm. Fig. 9(a), presents the recorded spectra for an PMMA based PNC film i.e. $YPO_4:Sm^{3+}$ (5 at. %) / PMMA film loaded with 10 wt.% NPs, along with pure PMMA film. The data reveal the emergence of a strong absorption band in the range of 200 nm to 225 nm for both the films. The increased absorption in the ultraviolet region has been previously reported in several studies, corresponding to the π-π^* transition of the carbonyl groups in PMMA [50], [51]. However, a slight increase in the intensity of this band is observed in the PNC film, attributed to the excitation of the charge transfer band (CTB) of the YPO_4 matrix [52]. A notable decrease in absorption intensity is observed between 225 nm and 260 nm, stabilizing beyond 260 nm. Nevertheless, a difference of approximately 11% is noted in the absorbance intensity for the NC $YPO_4:Sm^{3+}$ (5 at. %) /PMMA film, to the scattering of light in the visible region by the NPs encapsulated in the polymer. It has been demonstrated that $YPO_4:Sm^{3+}$ NPs absorb a portion of visible light in the range of 350-550 nm, unlike the pure PMMA film, which remains transparent in this wavelength range [52-53].

In Figure 9(b), includes UV-Vis spectra of the PS based PNC film i.e. YPO_4: Sm^{3+} (5 at. %) / PS, as well as a pure PS film. The appearance of an absorption peak in the UVB range (235-280 nm) in both films is generally attributed to lower-energy electronic transitions, which often correspond to the promotion of an electron from the highest occupied orbital to the lowest vacant orbital of polystyrene [31], [54]. Additionally, a slight red shift of the absorption peak accompanied by a decrease in intensity is worth noting in the case of the PNC YPO_4: Sm^{3+} (5 at.%)/PS. This behavior originates from the presence of $YPO_4:Sm^{3+}$ NPs in the polymer, thereby causing a reduction in the bandgap of the NC.

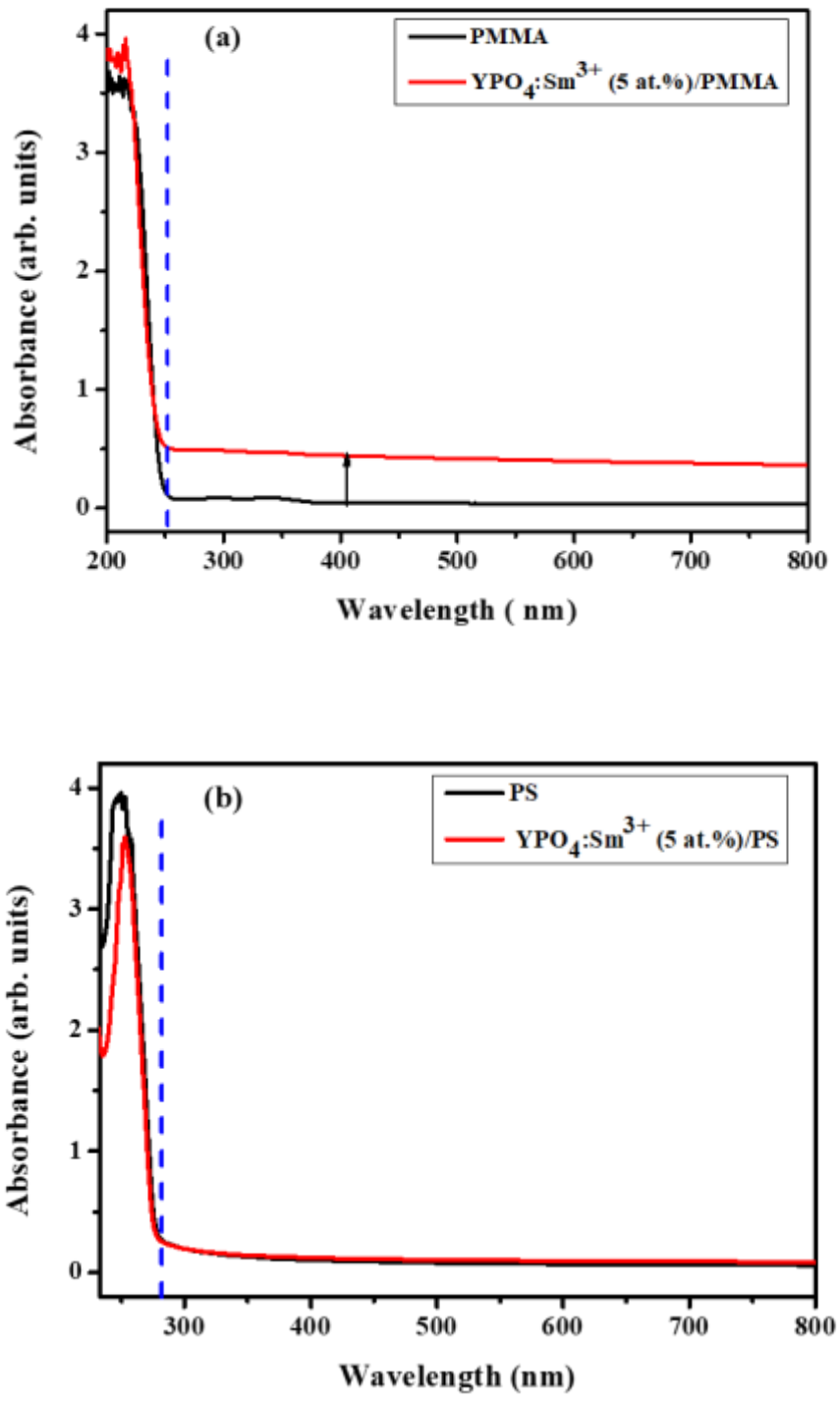

Fig. 9 UV-Vis absorbance spectra of (a) NC $YPO_4:Sm^{3+}$ (5 at. %)/PMMA along with pure PMMA films, (b) NC $YPO_4:Sm^{3+}$ (5 at. %) /PS along with pure PS

3.3. Photoluminescence spectroscopy

3.3.1. Photoluminescence investigation of YPO_4: Sm^{3+} nanopowders

In order to investigate the luminescent properties of YPO_4: Sm^{3+} (x at.%) nanopowders, the excitation and emission spectra were recorded. The excitation spectra of nanopowders were recorded at 300 -550 nm range at room temperature for an emission wavelength λ_{em}= 601 nm. As observed in the excitation spectra, multiple excitation peaks appear at similar wavelength positions for all samples, corresponding to characteristic intra-configurational electronic transitions ($4f^5$-$4f^5$) of Sm^{3+} ions [46, 55, 26]. The respective excitation wavelengths of these transitions, along with their identifications, are illustrated in Fig. 10. However, it is noteworthy that the peak at 404 nm, corresponding to the ($^6H_{5/2} \rightarrow {}^4F_{7/2}$) transition, exhibits maximum absorption, with a more pronounced intensity for the 5 at.% Sm^{3+} doped sample. Beyond this concentration, the intensity begins to decrease, as seen in the 8 at.% and 10 at.% Sm^{3+} doped samples. This reduction in intensity may be attributed to concentration quenching phenomenon of the activator ions in the YPO_4 matrix, this excess concentration will lead to exchange interactions between dopants (Sm^{3+}-Sm^{3+}) [56,57].

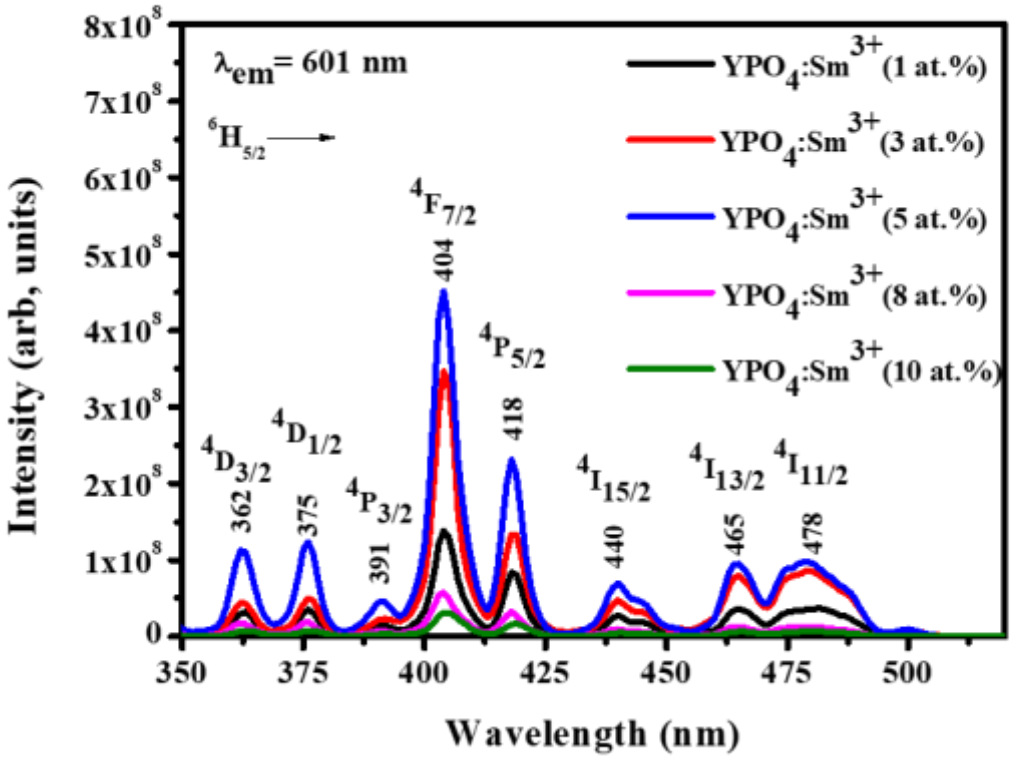

Fig. 10 Excitation spectra of the YPO_4:Sm^{3+} (x at. %) nanopowders under λ_{em} = 601 nm

The emission spectra of the YPO_4: Sm^{3+} nanopowders obtained under near-UV light at λ_{ex} = 404 nm are shown in Fig. 11(a). The recorded emission spectra of nanopowders consist of four bands in the range of (530 – 720nm) positioned at 561, 601, 643, and 704 nm, corresponding to orange-red emissions witch are attributed to the fluorescence from the $^4G_{5/2}$ level to the ^6H_J levels (J = 5/2, 7/2, 9/2, 11/2) [58, 59], as illustrated in the diagram presented by Fig. 11(b). The orange luminescence at 601 nm corresponding to $^4G_{5/2} \rightarrow {}^6H_{7/2}$ transition is the most dominant. Fig. 12(a) depicts the variation in integrated fluorescence intensity of $^4G_{5/2} \rightarrow {}^6H_{7/2}$ as a function of Sm^{3+} ion doping concentration. These results affirm that the 5 at.% concentration corresponds to an optimal amount of Sm^{3+} ions; beyond this value, the intensity decreases, this is commonly called ‘’concentration quenching’’ [60,25]. In other words, the distance between two identical Sm^{3+} activator centers decreases (critical distance), leading to non-radiative energy transfer, various interaction mechanisms such as exchange contact, multipole-multipole interaction between Sm^{3+} ions, and the self-reabsorption of light emitted by neighboring dopants all collectively contribute to this extinction phenomenon. To understand the nature of interaction between Sm^{3+} ions, the critical distance (Rc) is estimated using Blasse's equation [61].

$$R_C \sim 2.\left[\frac{3V}{4\pi.N.x_c}\right]^{1/3}$$

Where x_C symbolizes the critical concentration of the dopant ion, while N and V respectively represent the number of cations and the volume of the unit cell. In our case, these values are x_c= 0.05, V = 287.20 Å, N = 4 [52]. The critical distance between Sm^{3+} ions doped in YPO_4 phosphor was measured to be 10.45 Å. The value of R_C determines the type of interaction responsible for energy transfer. If R_C is greater than or equal to 5 Å, then energy transfer is governed by electric multipolar contact [53].

After identifying the interaction responsible for energy transfer (multipolar interaction), the next step is to determine the type of dipoles involved in this interaction. To achieve this, Huang developed an expression relating light intensity to the doping ratio of activating ions as follows [62]:

$$\log\left(\frac{I}{X}\right) = log\beta - \frac{S}{d}\, log(X) \qquad (4)$$

given that I and X represent the emission intensity and dopant concentration, respectively. β is a constant, and d is defined as equal to 3 (the compound's dimension). It is assumed that energy transfer occurs between Sm^{3+} ions within the NPs. Here, s represents the crucial parameter determining the type of dipoles involved, which can take three distinct values [62], [63]:

$$\text{If } s = \begin{cases} 6 & \text{dipole} - \text{dipole interactions} \\ 8 & \text{dipole} - \text{quadrupole interactions} \\ 10 & \text{quadrupole} - \text{quadrupole interactions} \end{cases}$$

The value 's' is calculated by utilizing the slope of the linearly fitted curve log (I/x) as function log(x). The result is illustrated in the Fig. 12(b).

The deduced value of s, which is 6,6 and close to 6, suggests that the dipole-dipole nature of concentration transfer between Sm^{3+} ions in YPO_4 phosphors is responsible. In conclusion, the investigation into the photoluminescence properties of YPO_4: Sm^{3+} nano-phosphors suggests that it is a suitable material for use in the field of optoelectronics, specifically in orange-red LED display technology.

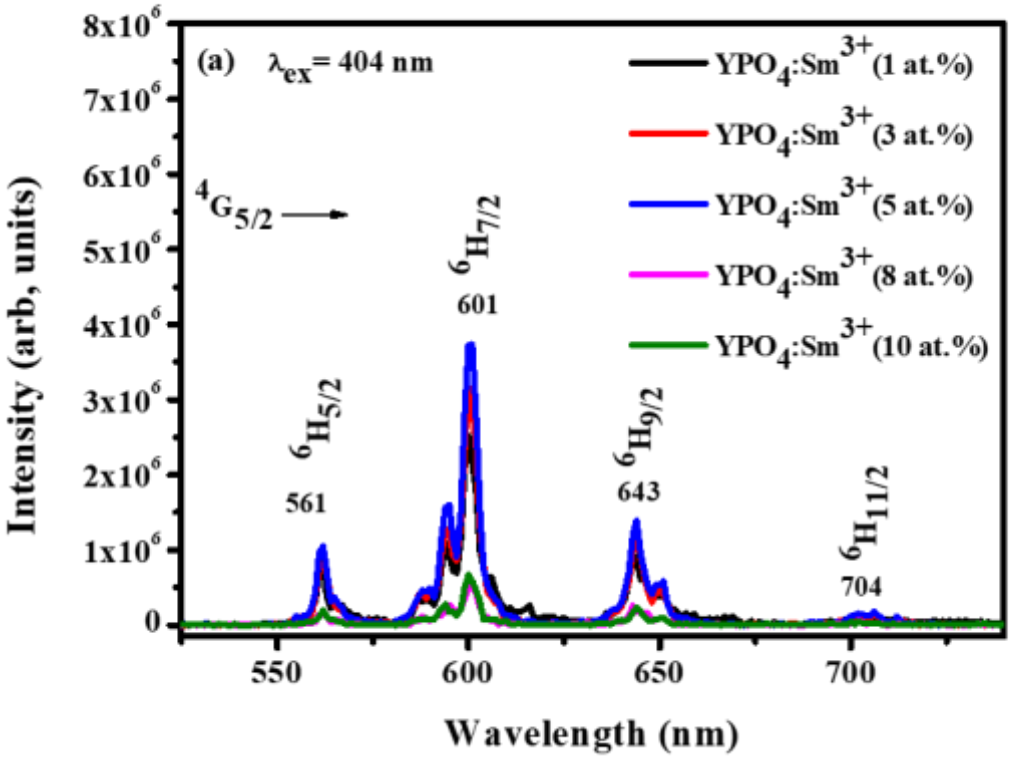

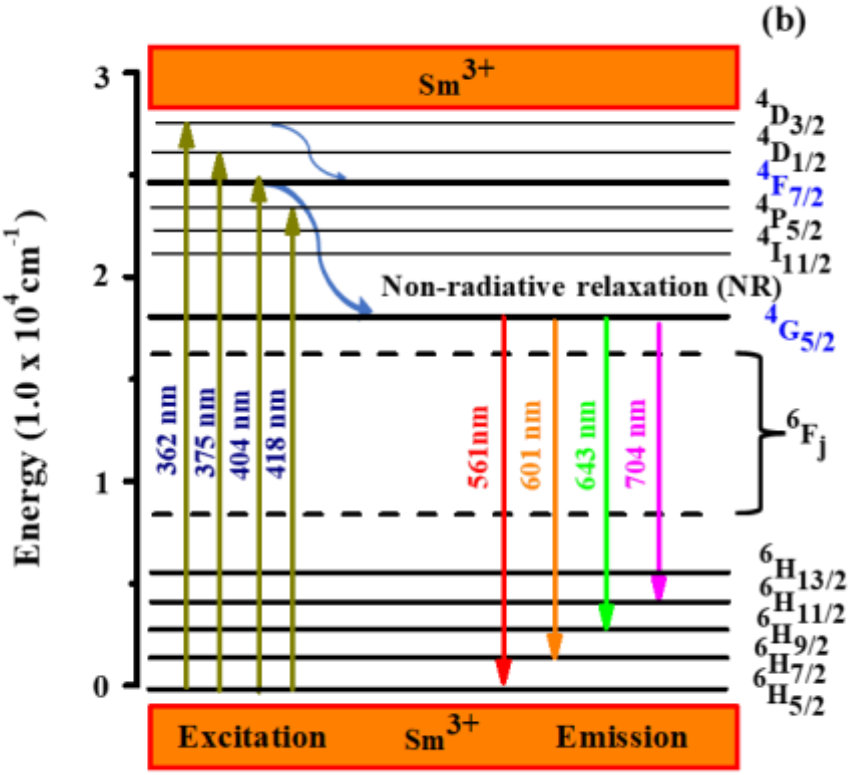

Fig. 11 (a) Emission spectra of the $YPO_4:Sm^{3+}$ (x at. %) nanopowders under λ_{ex} = 404 nm , (b) Explanatory diagram of observed fluorescence transition

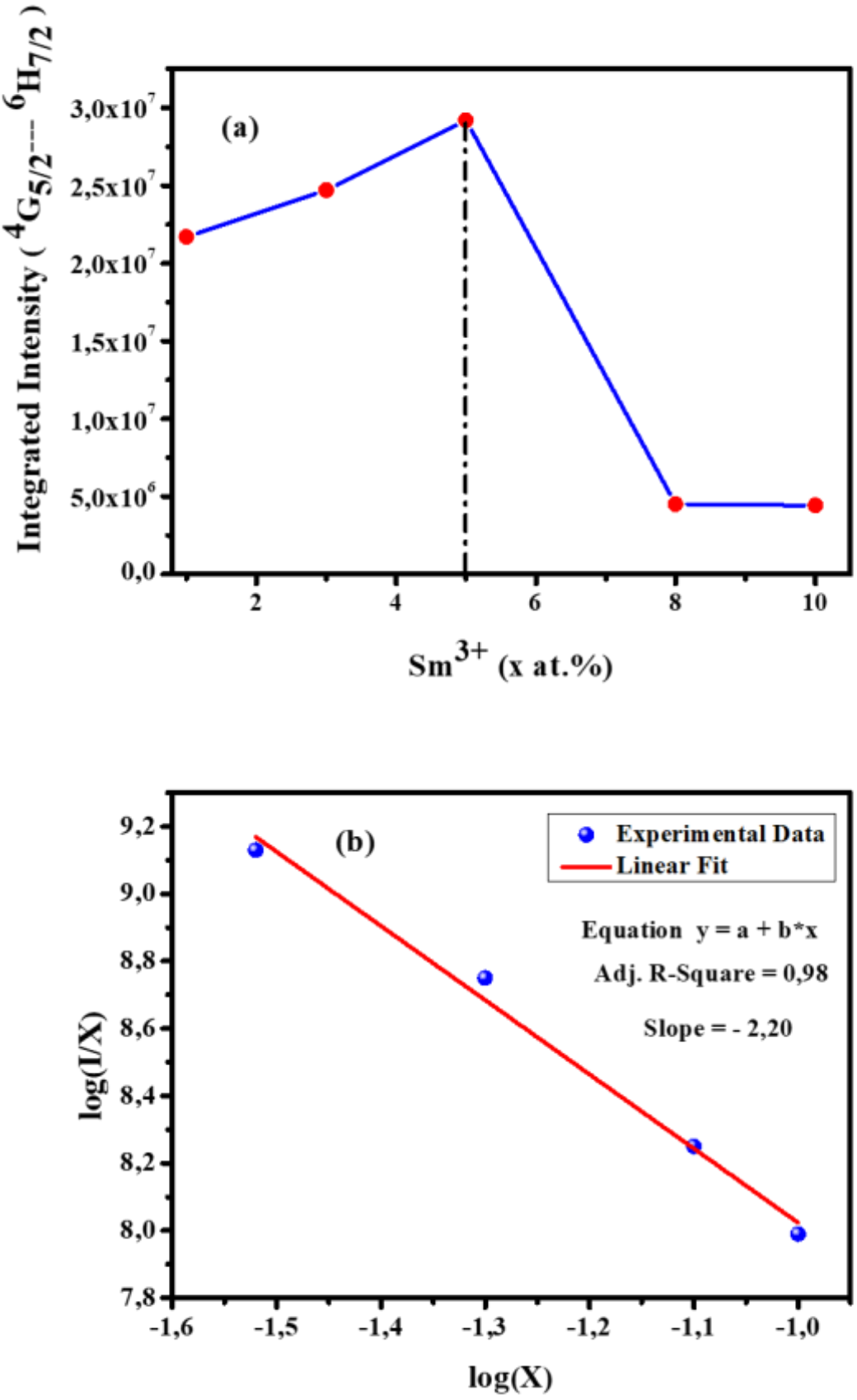

Fig. 12 (a) Integrated fluorescence intensity of $^4G_{5/2}$—$^6H_{7/2}$ as a function of Sm^{3+} ion doping rate, (b) log(I/x) versus log(x) plot of nano-phosphors YPO_4: Sm^{3+} (x at. %)

3.3.2. Photoluminescence investigation of YPO_4 : Sm^{3+} based PNC films

Recently, the widespread use of organic materials such as PS and PMMA has expanded into various technological applications.

As discussed above, PNCs films based on PMMA and PS polymers were synthesized using the direct blending process in solution with a 10 wt.% content of YPO_4:Sm^{3+}(5 at.%) nanophosphors. Luminscence response study through photoluminescence characterization of the synthesized films was conducted, recording excitation and emission spectra.

Fig. 13 (a, b) shows the emission spectra of PS and PMMA polymer films recorded in the UV-Vis range at room temperature under UV excitation at 325 nm. The PMMA film exhibits a broad emission band spanning from the near UV to the visible range, from 350 to 600 nm. Kara et al. highlighted this emission across a wide spectrum for PMMA following UV excitation at 349 nm in their paper, stating that it is attributed to π*--π or n*---- π intra-ligand charge transfer transitions [64]. The emission spectrum of the PS revealed a broad and intense emission band in the UVA region (340-400 nm) as shown in Fig. 12 (b). This emission band is attributed to the presence of organic impurities acting as luminescence activators, such as 2,5-Diphenyloxazole (PPO) and POPOP (1,4-bis(5-phényloxazol-2-yl) benzene) , embedded in the polystyrene composition, serving as a luminescence booster in the plastic films [65-66].

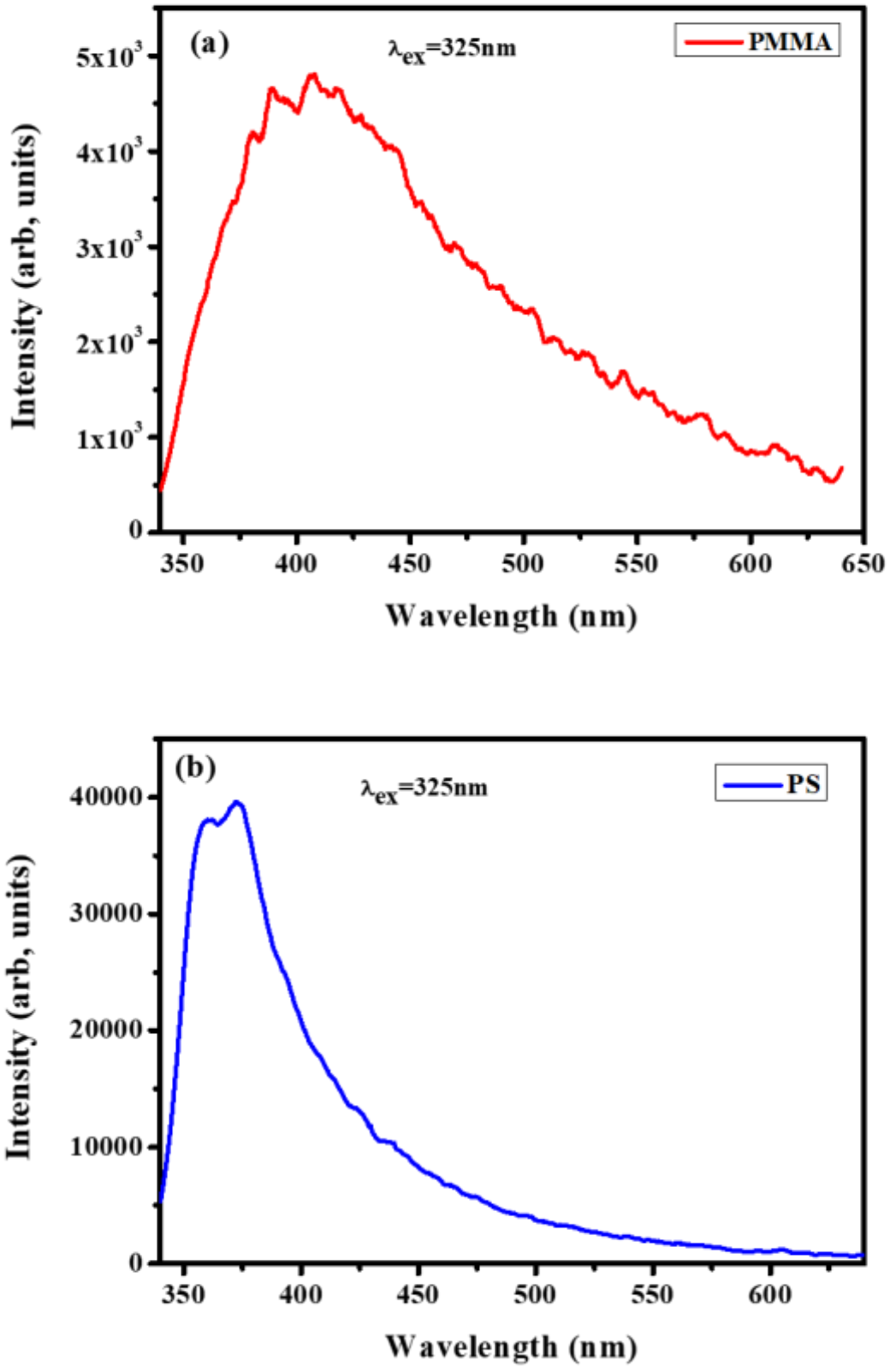

Fig. 13 Emission spectra under UV excitation at 325 nm of pure (a) PMMA and (b) PS films

The excitation and emission spectra of the PNCs films were recorded under the same wavelength conditions as used for the spectra of the $YPO_4:Sm^{3+}$ nanopowders.

Fig. 14(a, b) illustrates the excitation spectra of PMMA based PNCs i.e. YPO_4: Sm^{3+}/PMMA and PS based PNCs i.e. YPO_4: Sm^{3+}/PS NC films recorded at room temperature under $\lambda_{em} = 601\text{nm}$. The obtained emission spectrum of PNC films presents the same profiles as the $YPO_4:Sm^{3+}$ (5 at.%) nanopowder (see Fig.10). All observed excitation band are characteristic to $4f^5$ ($^6H_{5/2}$)→$4f^5$ transitions of Sm^{3+} ions [53]. However, no excitation peaks were observed for pure PS and PMMA films in the 350-500 nm range given that these polymers are transparent in the near-UV-Vis region.

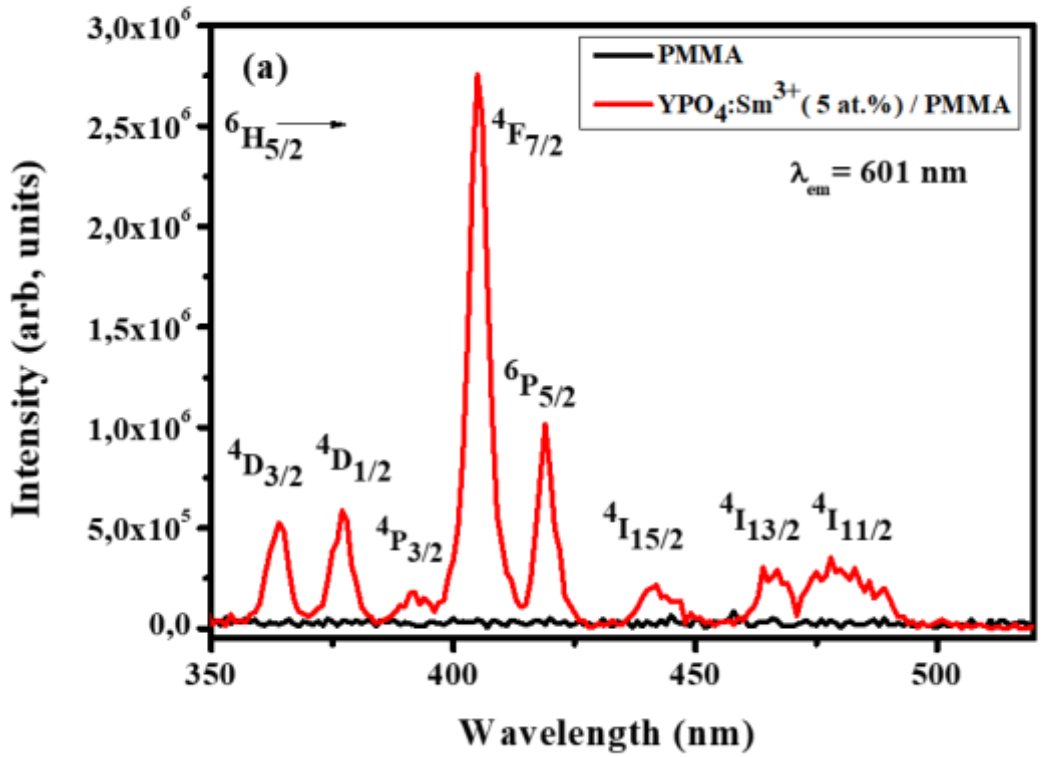

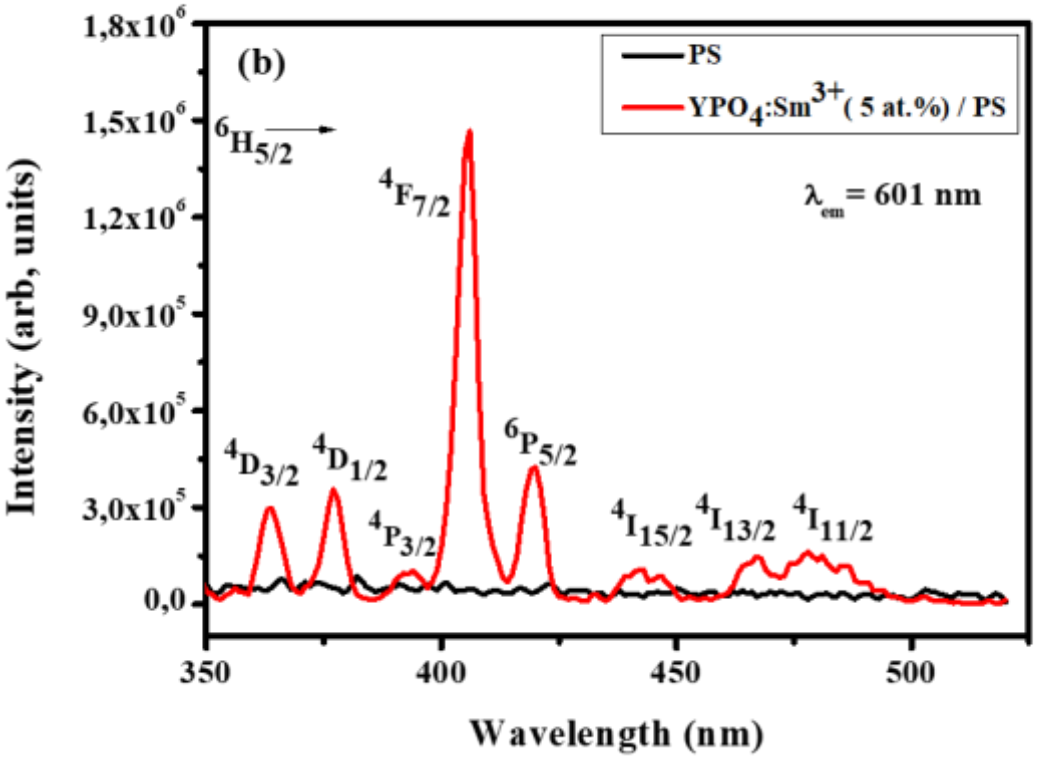

Fig. 14 Excitation spectra of (a) YPO_4: Sm^{3+}/PMMA and pure PMMA films (b) YPO_4: Sm^{3+}/PS and pure PS films.

The emission spectra of PNCs films were recorded under near-UV excitation at 404 nm, Fig. 15(a,b). The emission peaks observed at 561 nm, 601 nm, 643 nm, and 704 nm are attributed to the interconfigurational luminescence of the Sm^{3+} ions from the radiative transitions from the $^4G_{5/2}$ level to the ^6Hj series (j = 5/2, 7/2, 9/2, 11/2) [56]. These emission peaks of YPO_4: Sm^{3+} NPs kept their position in YPO_4: Sm^{3+}/PMMA and YPO_4: Sm^{3+}/PS PNCs films.

It should be noted that the luminescence transition from the $^4G_{5/2}$ level to the $^6H_{7/2}$ level at 601 nm (orange emission) exhibits optimal intensity in the visible region. However, no intrinsic luminescent signature associated with the polymer matrix was detected, confirming the results predicted by the previously mentioned UV-Vis analysis. As for the relative emission intensities of the two nanocomposites, the YPO_4: Sm^{3+}/PMMA film stands out more significantly. This difference could be attributed to the crystalline quality of the nanocomposite films, which could be influenced by the distribution and the charge ratio of NPs within the polymer matrix. It has been demonstrated that in hybrid systems involving the interface between polymers and nanoparticles, it is possible to observe exchange of energy and charge carriers, which can influence the luminescence properties of the resulting material

[67-68]. In summary, the photoluminescence properties and UV-Vis spectroscopy of both polymers indicates that PS and PMMA matrices provide an ideal environment for fabrication of $YPO_4:Sm^{3+}$ /polymer nanocomposite phosphors films.

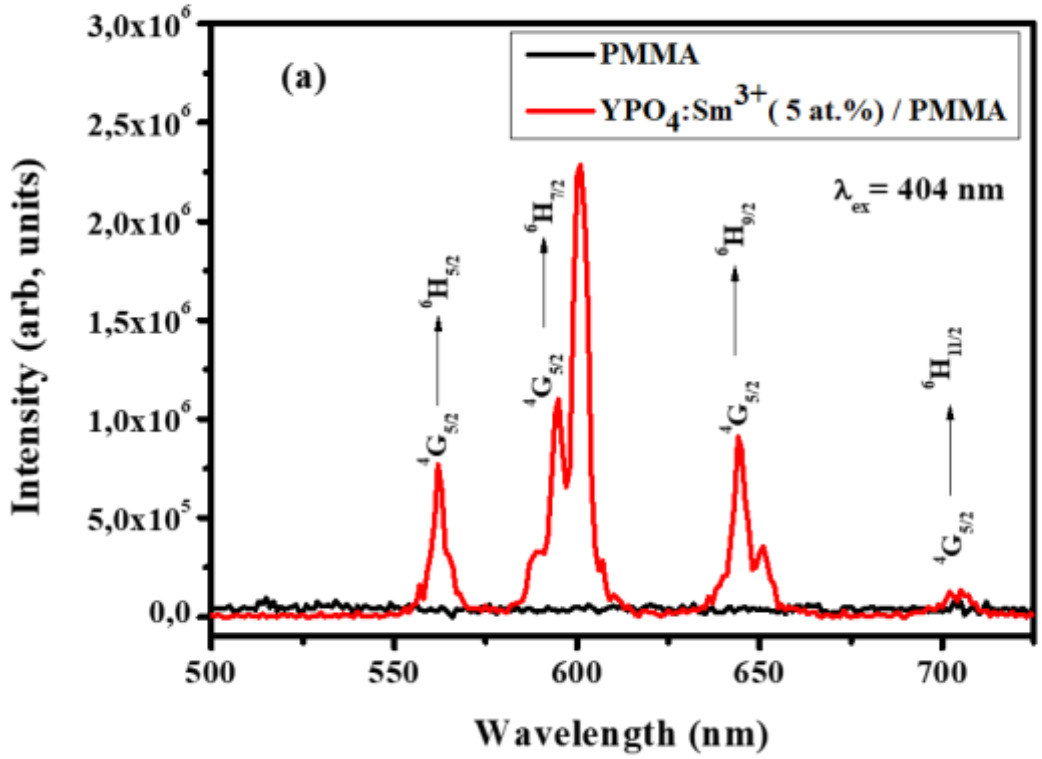

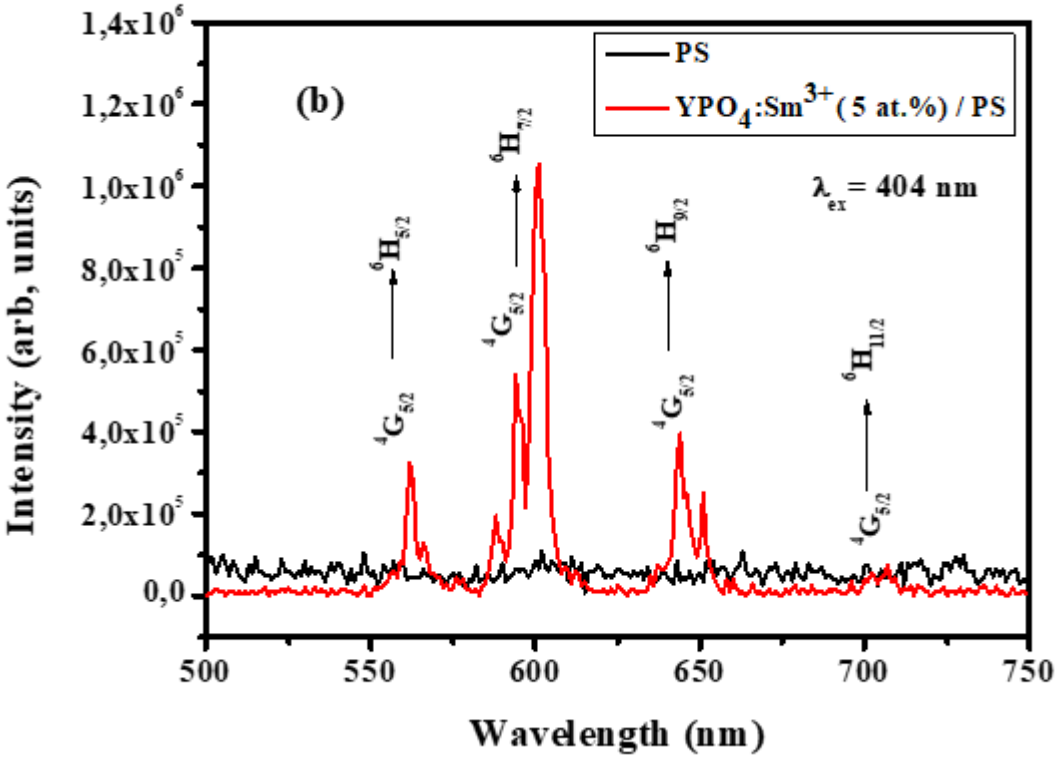
(b)
PS
YPO4:Sm3+ (5 at.%) / PS
λex = 404 nm
6H5/2
4G5/2
6H7/2
4G5/2
6H9/2
4G5/2
6H11/2
4G5/2
Intensity (arb, units)
Wavelength (nm)

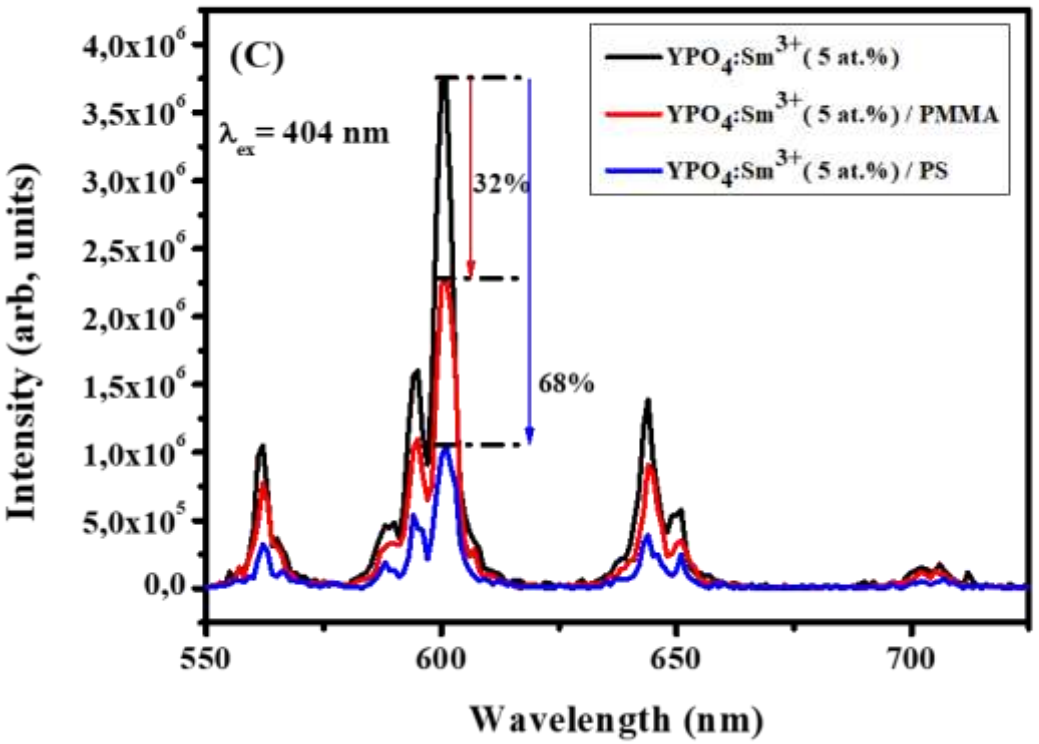
(C)
λex = 404 nm
YPO4:Sm3+ (5 at.%)
YPO4:Sm3+ (5 at.%) / PMMA
YPO4:Sm3+ (5 at.%) / PS
32%
68%
Intensity (arb, units)
Wavelength (nm)

Fig. 15 Emission spectra of (a) YPO_4: Sm^{3+}/PMMA PNC and pure PMMA films, (b) YPO_4: Sm^{3+}/PS PNCs and pure PS films, (c) Comparison of the emission intensity of PNC films with the emission of the YPO_4:Sm^{3+} nano-phosphor under excitation at 404 nm.

Moreover, referring to the results reported in Fig. 15(c), the incorporation of YPO_4:Sm^{3+} into the polymer matrix led to a decrease in emission intensity of approximately 32% when incorporated into the PMMA matrix, and 68% in the PS matrix. This behavior has been observed in several similar research studies [21-69], indicating that this loss of intensity refers to two common phenomena in NCs: the bathochromic effect and the hypochromic effect due to the lower refractive index of the polymers compared to that of the incorporated NPs [21]. In some cases, a higher refractive index can increase the probability of reabsorption and reemission in the PNC film, affecting the spectral purity and overall intensity of photoluminescence. Part of the emitted light is reabsorbed and may not be reemitted, which can also lead to non-radiative losses.

3.3.3. Temperature-dependent photoluminescence (TDPL)

Given that the thermal stability of phosphors is recognized as crucial for their practical applications, particularly in high-power lighting and displays, it presents a key technical parameter. With this in mind, the thermal stability of nano-phosphor YPO_4: Sm^{3+} (5 at. %) in its solid-state and subsequently in PMMA polymer film was evaluated. Fig. 16(a) shows the emission spectra of nano-phosphor YPO_4: Sm^{3+} (5 at. %) recorded under excitation at 404 nm at different temperatures ranging from 100 K to 400 K. The initial observation reveals that the position and shape of the peaks remain unchanged. However, the emission intensities slightly change with temperature variation. This change is illustrated in Fig. 16(b). Over the temperature range from 100 K to 400 K, the relative emission intensities show a general trend of decreasing with increasing temperature. Specifically, from 100 K to 300 K, the emission intensities gradually increase as the temperature decreases. At 200 K and 100 K, they are 13% and 46% higher, respectively, than the emission of YPO_4: Sm^{3+} (5 at. %) nanophosphor at room temperature. Then, from 300 K to 400 K, the emission intensities decrease with increasing temperature, with a decrease of 8% at 350 K and 23% at 400 K compared to the luminescence of the nanophosphor at room temperature. This reduction in light intensity is often associated with a phenomenon of thermal quenching induced by temperature, this

property is crucial for numerous phosphor applications, where thermal quenching is only supposed to be significant above 300 K to maintain effectiveness at room temperature [70]. In modern LED lighting, phosphors like Ce^{3+} doped garnet $Y_3Al_5O_{12}$ typically function at temperatures near 100 °C, avoiding early degradation. For high-power white light-emitting phosphors (WLEDs), thermal stability of at least 200 °C is essential. Moreover, this thermal decrease in emission intensity and/or decay time is employed in thermometry as well [71, 72]. In general, luminescence excitation occurs through two main mechanisms: multiphonon relaxation, which depends on the nature of the host matrix and the type of emitting center (RE), or through a crossing mechanism. In our case, the energy gap between the $^4G_{5/2}$ fluorescent level and the lower $^6F_{11/2}$ level of Sm^{3+} ions is approximately 7421 cm^{-1}[73], nearly six times the phonon energy of the YPO_4 matrix, which is around 1080 cm^{-1}. Consequently, excitation via multiphonon relaxation generally cannot occur. Therefore, the main reason for thermal quenching in this material is due to the crossing process, and the overall variation in luminescence intensity with temperature can be explained by the following Arrhenius formula [73], [74]:

$$\frac{I_T}{I_0} = [1 + \gamma . Exp(-\Delta E/k_B T]^{-1} \qquad (5)$$

Where I_0 and I_T are luminescence intensity of YPO_4: Sm^{3+} (5 at. %) at room temperature and the testing temperature respectively. γ is a constant, k_B is Boltzmann constant (8.62 $x10^{-5}$ eV /K). The obtained result (Fig. 16(c)), reveals an activation energy ΔE of 0.296 eV. This relatively high activation energy suggests that YPO_4: Sm^{3+} (5 at. %) exhibits promising thermal stability at a temperature of 400 K, our nanophosphor demonstrates an emission intensity that is 77% of the original emission intensity at room temperature.

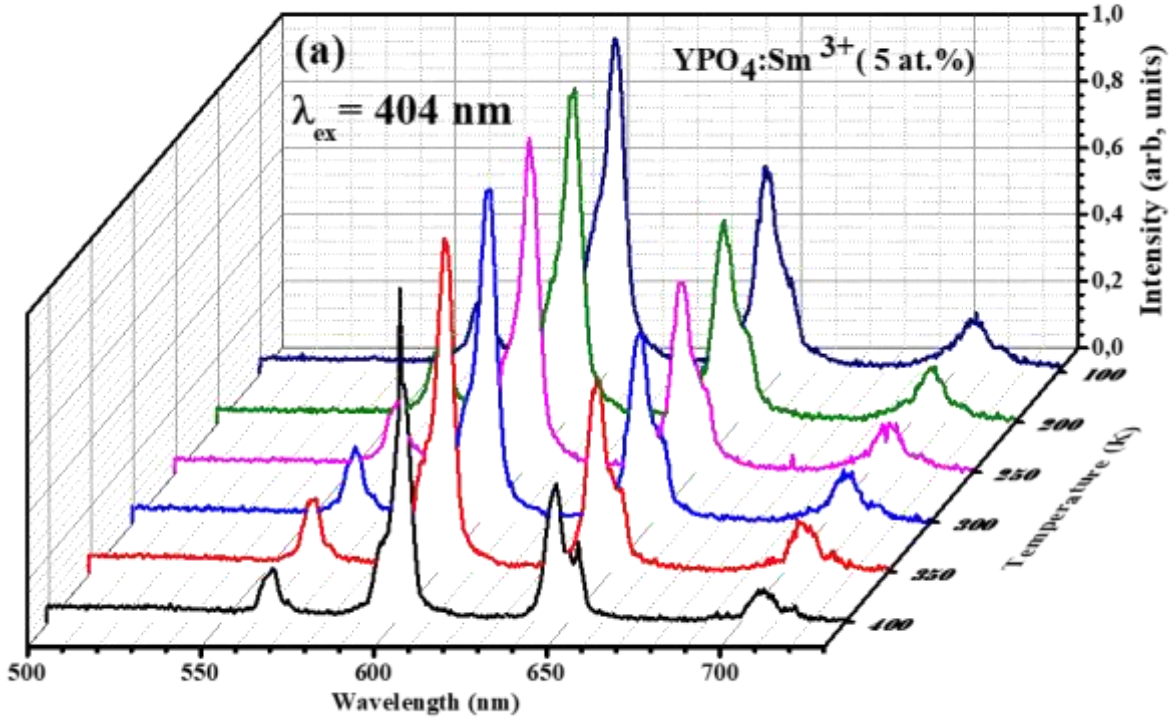
(a)
λex = 404 nm
YPO4:Sm 3+(5 at.%)
Intensity (arb, units)
1,0
0,8
0,6
0,4
0,2
0,0
100
200
250
300
350
400
Temperature (K)
500
550
600
650
700
Wavelength (nm)

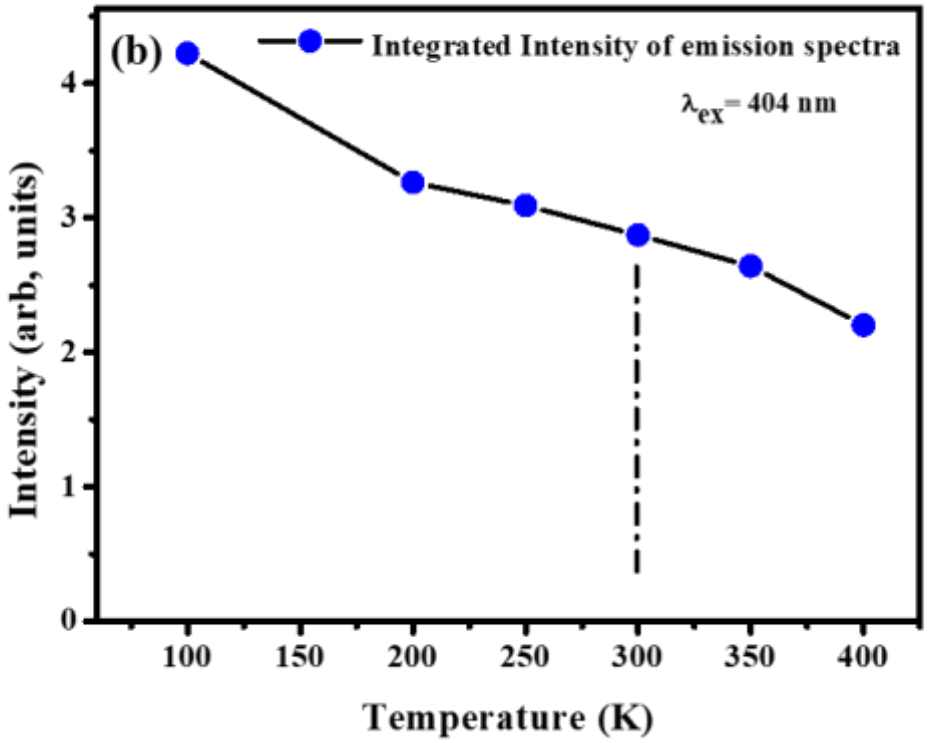
(b)
Integrated Intensity of emission spectra
λex= 404 nm
Intensity (arb, units)
0
1
2
3
4
100
150
200
250
300
350
400
Temperature (K)

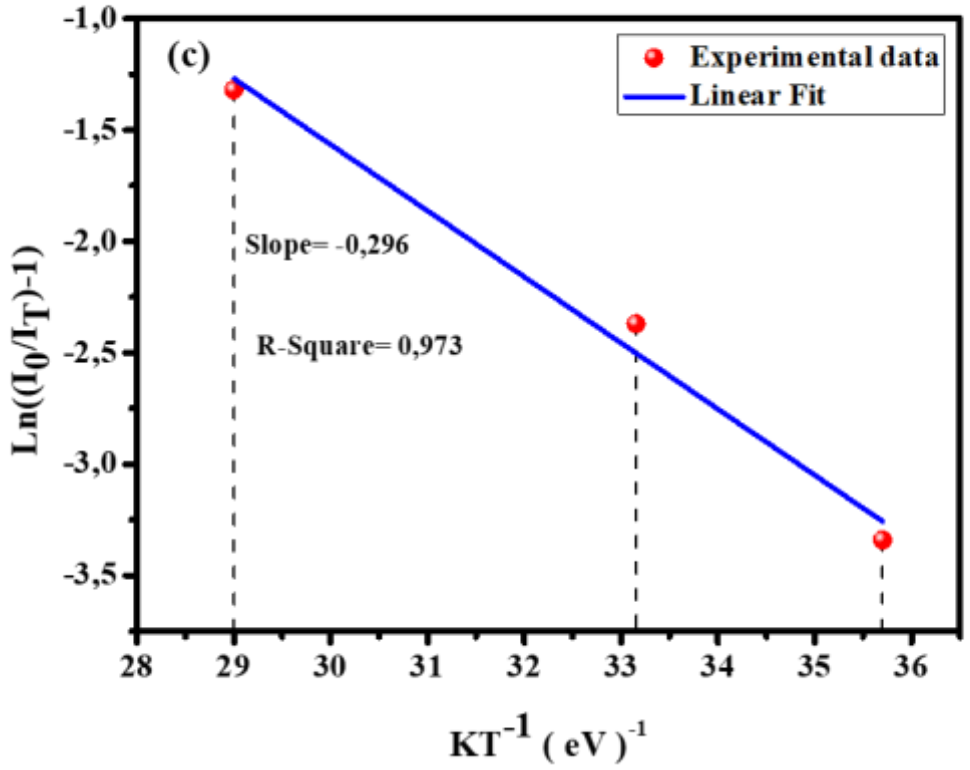

Fig. 16 (a) Emission spectra of YPO_4: Sm^{3+} (5 at. %) under excitation at 404 nm at different temperatures, (b) The integrated emission intensity as a function of temperature (100-400 K), (c) Plot of ln[(I_0/I) - 1] versus 1/(kT) of YPO_4: Sm^{3+} (5 at. %) nano-phosphor

We also explored the thermal stability of the YPO_4:Sm^{3+} nanophosphor within a PMMA polymer. Thus, we have depicted in Fig. 17(a) the photoluminescence spectra of YPO_4: Sm^{3+} (5 at.%) /PMMA PNC film under excitation at 404 nm at different temperatures ranging from 75 K to 400 K. The results revealed no shift in the position of emission peaks, indicating that the YPO_4:Sm^{3+} NPs maintain their luminescence purity within the polymer. However, a change in intensity was observed as the temperature varied as shown in Fig. 17(b). Over the temperature range from 75 K to 400 K, the luminescence intensity consistently decreases as the temperature increases. Specifically, from 75 K to 300 K, the luminescence intensity increases with decreasing temperature, showing a notable rise of approximately 36% at 150 K and 65% at 75 K compared to the luminescence intensity of the NC film at room temperature (300 K). In the temperature range between 300 K and 400 K, the emission intensities decrease with increasing temperature due to the thermal quenching effect, with a decrease of 9% at 350 K and 22% at 400 K compared to the luminescence intensity at room temperature. We

maintain that the PMMA polymer exhibits no reactions that could compromise the emission properties of the $YPO_4:Sm^{3+}$(5 at. %) /PMMA film when subjected to temperature variations, demonstrating its excellent performance in terms of thermal stability. Thus, offering the promising support for luminescent nanomaterials.

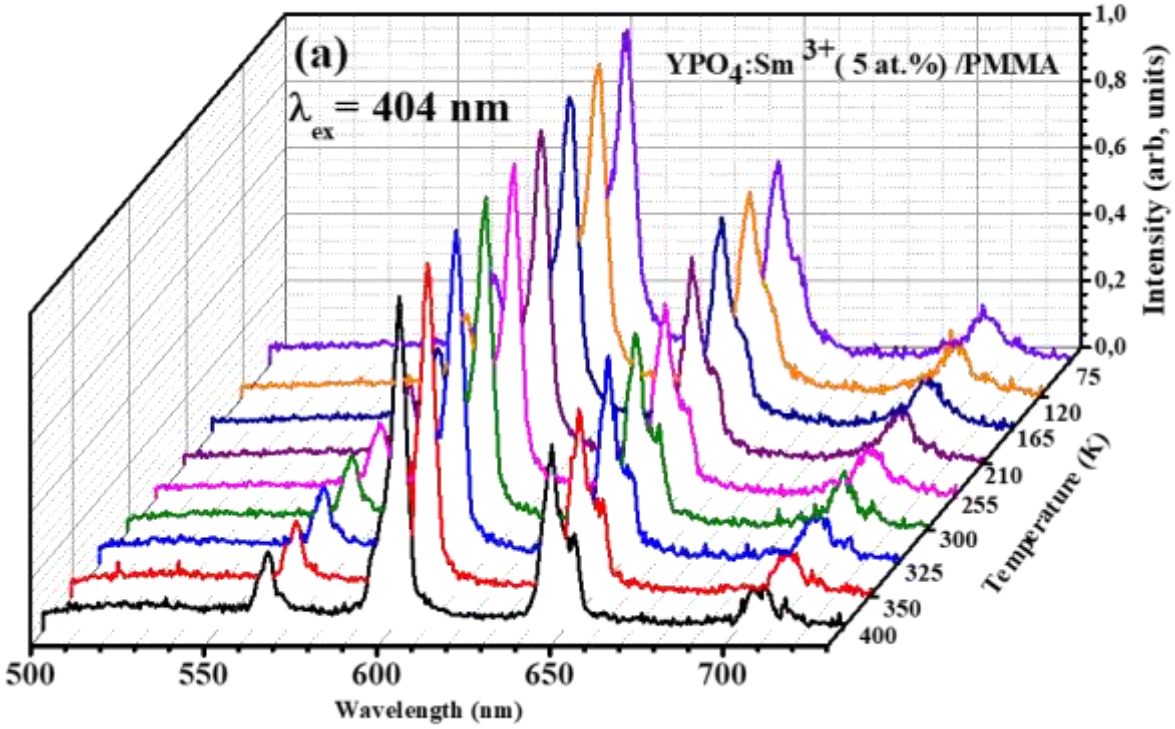

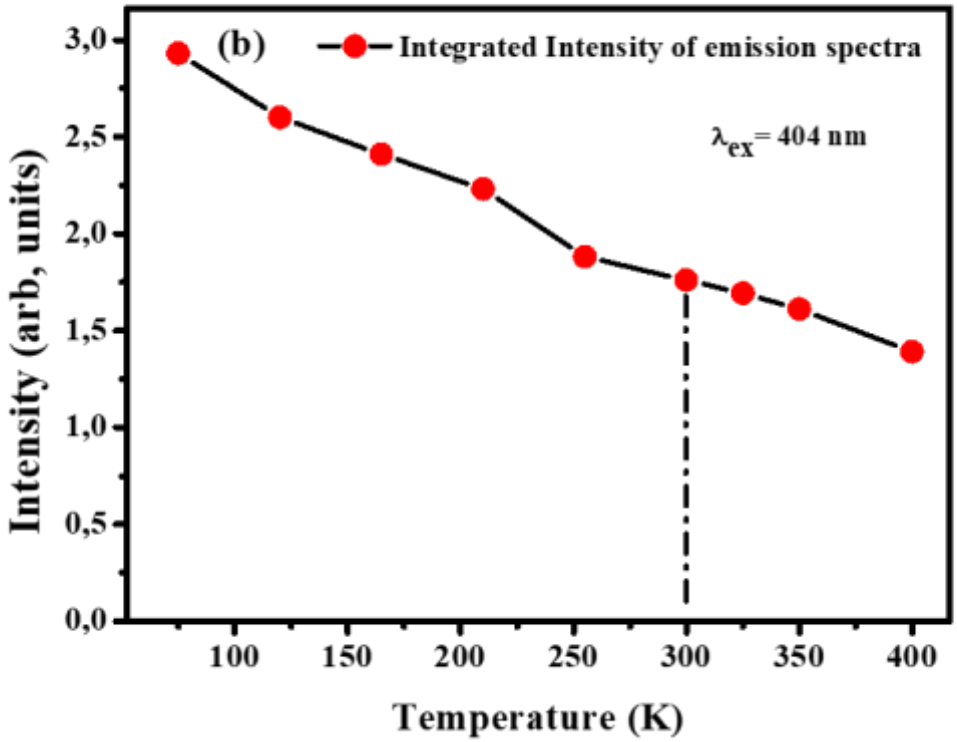

Fig. 17 (a) Emission spectra of YPO_4: Sm^{3+} (5 at. %) / PMMA under excitation at 404 nm at different temperatures, (b) The integrated emission intensity as a function of temperature (75-400 K**)**

3.3.4. Luminescence decay curves

Fluorescence lifetime (decay lifetime) is one of the important parameters to study the properties of phosphors. The PL decay curves for both YPO_4:Sm^{3+} nanopowders and YPO_4:Sm^{3+}/PNC films were measured at room temperature, under emission wavelength at 601 nm and excitation at 404 nm, as illustrated in Fig.18. The emission decay curves were fitted with mono-exponential decay equation [75]:

$$I_t = I_0 + \Gamma . Exp\left(-\frac{t}{\tau}\right) \qquad (6)$$

where I_t and (I_0+ Γ) are the PL intensity at time t and at t = 0, respectively. Γ represents the magnitude of the emission intensity at t = 0 and I_0 is the detector background signal, while τ signifies the decay lifetime.

The values of τ for each of the nano-powders $YPO_4:Sm^{3+}$ and NCs films have been estimated and compiled in Table. 3.

Table. 3 Luminescence decay lifetime of $^4G_{5/2} \rightarrow {}^6H_{7/2}$

Samples	lifetime τ(ms)
YPO_4: Sm^{3+} (1 at. %)	2.16
YPO_4: Sm^{3+} (3 at. %)	2.07
YPO_4: Sm^{3+} (5 at. %)	1.74
YPO_4: Sm^{3+} (8 at. %)	1.36
YPO_4: Sm^{3+} (10 at. %)	1.10
YPO_4: Sm^{3+} (5 at. %)/PS	1.46
YPO_4: Sm^{3+} (5 at. %)/PMMA	1.27

It is observed that the fluorescence lifetime of the $^4G_{5/2}$ level decreases as the concentration of Sm^{3+} increases in YPO_4 nanopowder as shown in Fig. 18(a) and Fig.19. This decrease could be attributed to the reduction in distance between Sm^{3+}-Sm^{3+} ions, thereby favoring an energy transfer mechanism and consequently shorter luminescence durations. Furthermore, the fluorescence decay from $^4G_{5/2} \rightarrow {}^6H_{7/2}$ in the nanocomposite films (Fig. 18(b-c)) is shorter than that in the original YPO_4 nanopowder (with 5 at. % Sm^{3+}), likely due to some weak interaction with the polymer matrix [77]. However, encapsulating the active Sm^{3+} ions in the nanocrystalline environment of YPO_4 should shield the ions against parasitic interaction with the highly energetic phonons of the polymer host, while this decrease in decay time is more likely due to an increase in effective refractive index [31,76], as the refractive index of PS and PMMA is higher than that of air. R. Meltzer et al. [78] observed similar behavior in their study on the dependence of fluorescence lifetimes of $Y_2O_3:Eu^{3+}$ NPs on the surrounding medium. They noted that when the particles are much smaller than the wavelength of light, the local electric field suffered by RE^{3+} is influenced by both the medium inside the NPs and the surrounding medium.

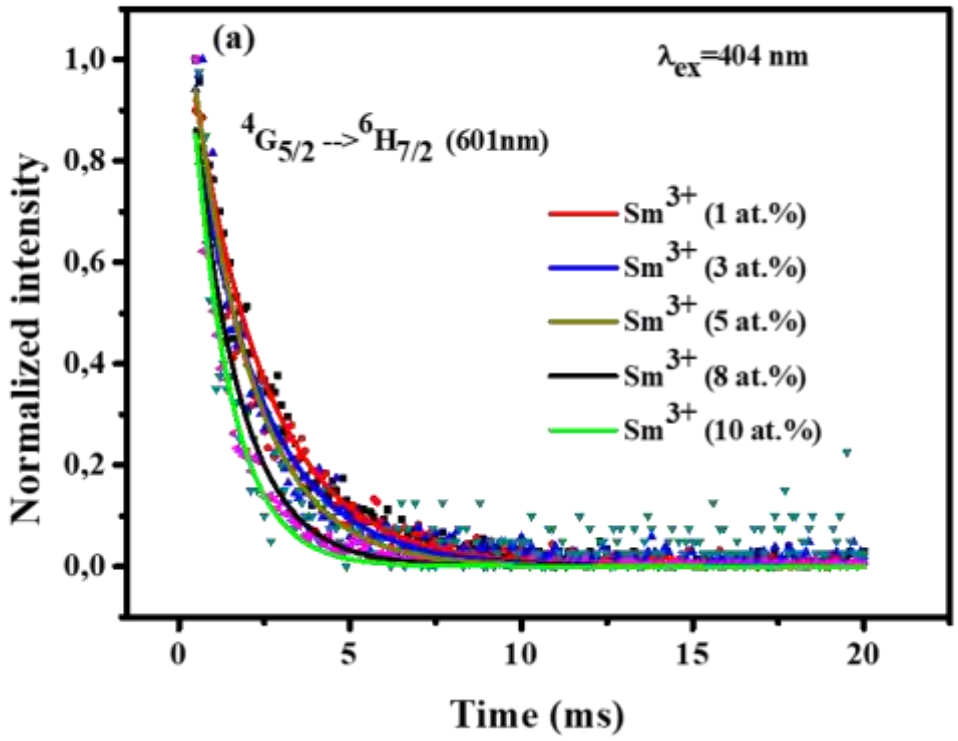
(a)
λex=404 nm
4G5/2 -->6H7/2 (601nm)
Sm3+ (1 at.%)
Sm3+ (3 at.%)
Sm3+ (5 at.%)
Sm3+ (8 at.%)
Sm3+ (10 at.%)
Normalized intensity
1,0
0,8
0,6
0,4
0,2
0,0
0
5
10
15
20
Time (ms)

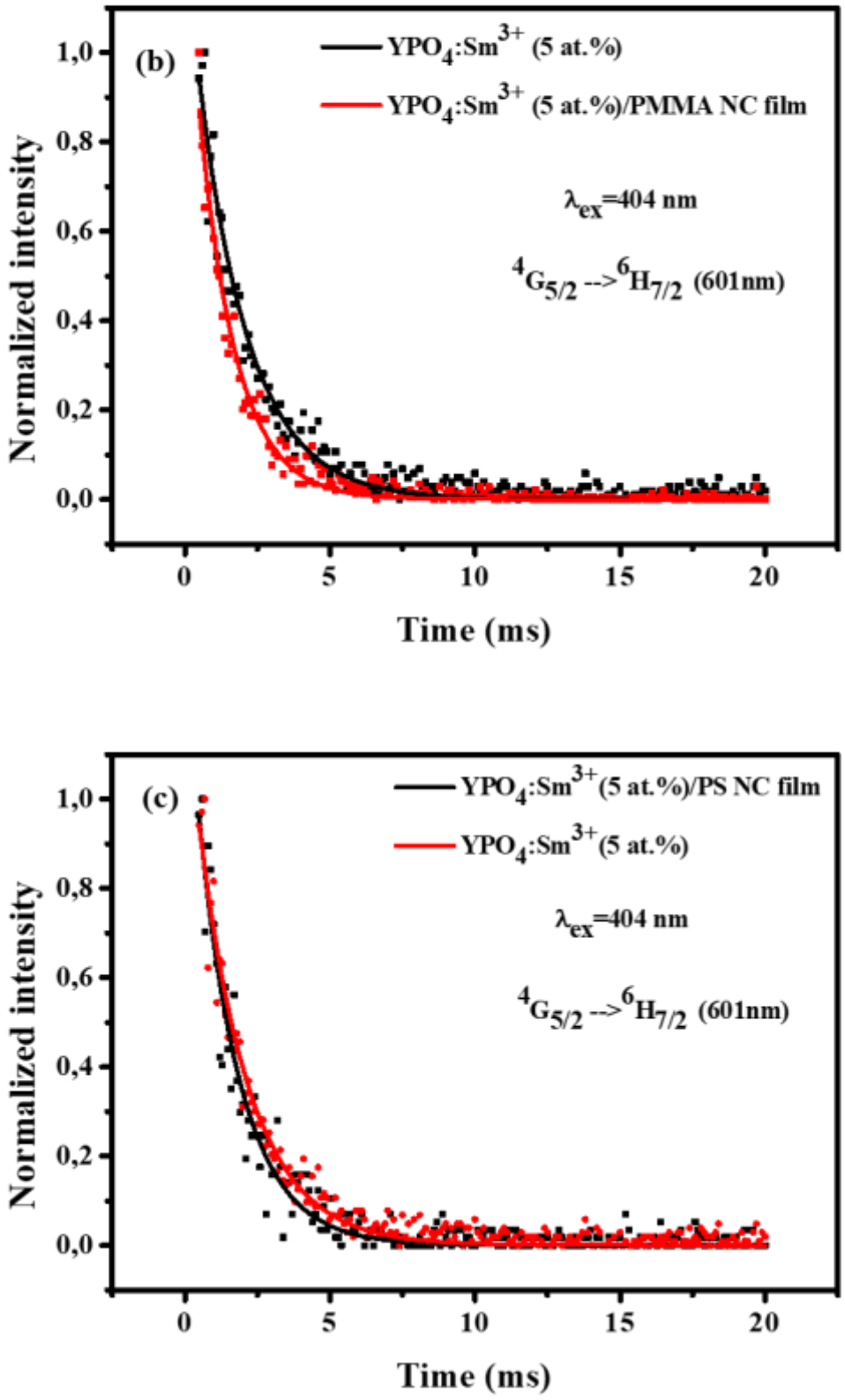

Fig. 18 Decay time curves of: (a)$YPO_4:Sm^{3+}$ nanopowders, (b) $YPO_4:Sm^{3+}$/PMMA NC film, (c) $YPO_4:Sm^{3+}$/PS NC film.

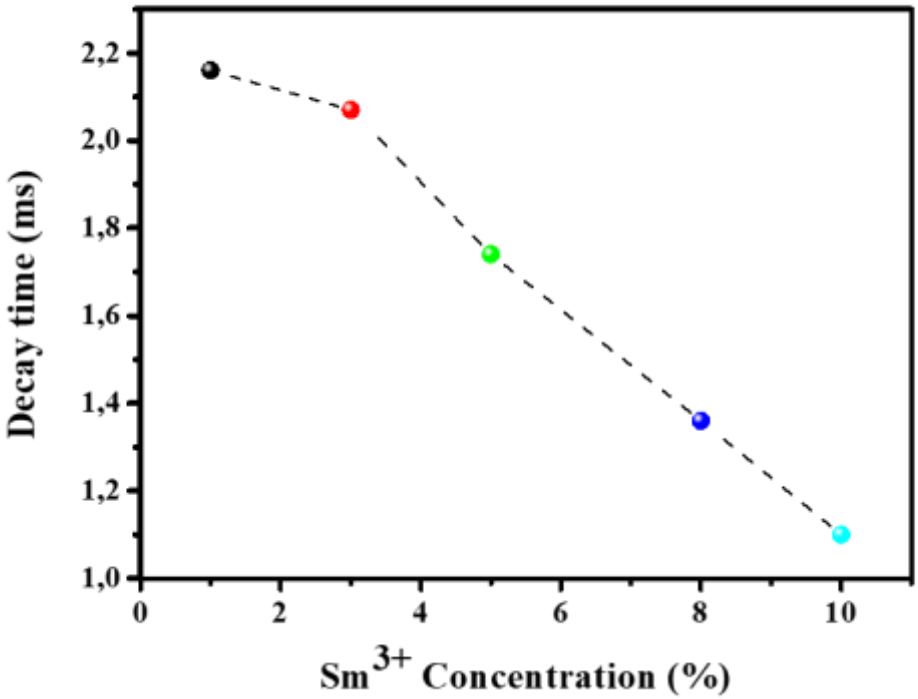

Fig. 19 Decay time versus Sm^{3+} concentration.

The connection between light and nanophosphors heavily hinges on the refractive index of these materials. Here, we have determined the refractive index of YPO_4:Sm^{3+} (x at. %) nanoparticles in both air and polymer mediums, employing the methodology outlined by Krsmanovic et al. [79]. The radiative lifetime of electric dipole (ED) transitions for an ion within a medium can be represented as [78]:

$$\tau_r = \frac{1}{f(ED)} \frac{{\lambda_0}^2}{[1/(3n^2+2)]^2 n} \qquad (7)$$

Where $f(ED)$, is the oscillator strength for the ED transition, λ_0 is the wavelength in vacuum and n is the refractive index of the medium.

When the NPs surrounded by the medium with a refractive index n_{med}, it is necessary to introduce an effective refractive index for the medium n_{eff}, which is given by [78]:

$$n_{eff}(x) = x n_{bulk} + (1-x) n_{med} \qquad (8)$$

Where x is the optical filling factor given by [78]:

$$x_{sample} = \frac{n_{samples} - n_{med}}{n_{bulk} - n_{med}} \qquad (9)$$

For instance, $n_{samples}$ denote the effective refractive index of nanoparticles (NPs) submerged in a medium with a refractive index n_{med}. This value can be calculated using the equation provided in reference [78]:

$$\frac{\tau_{bulk}}{\tau_{sample}}(n_{bulk}^2 + 2)^2 n_{bulk} = n_{sample}^5 + 4n_{sample}^3 + 4n_{sample} \qquad (10)$$

Using the reported $^4G_{5/2} \rightarrow {}^6H_{7/2}$ lifetime value by Enrico Cavalli τ(bulk) = 2.125 ms [81], measured under conditions similar to the current study for YPO_4: Sm^{3+} (5 at.%) in bulk, we calculated the effective refractive index (n_{eff}) for YPO_4: Sm^{3+} (5 at.%) nanoparticles surrounded by air, both in the case of nanopowder, with $n_{med}=n_{air}=1$, and in the case of YPO_4: Sm^{3+} (5 at.%) /PMMA and YPO_4: Sm^{3+} (5 at.%) /PS films, with $n_{med}=n_{PMMA}=1.49$ or $n_{med}=n_{PS}=1.67$ [80, 82], knowing that the bulk refractive index (n_{bulk}) for YPO_4 is 1.72 [83]. The values of n_{eff} are determined and presented in Table. 4.

Table. 4 Effective refractive index (n_{eff}) of YPO_4:Sm^{3+} NPs

Samples	$\tau\ (ms)$	n_{eff}
YPO_4:Sm^{3+}(5 at. %) NPs	1.74	1.82
YPO_4:Sm^{3+}(5 at. %)/PS NC film	1.46	1.91
YPO_4:Sm^{3+}(5 at. %)/PMMA NC film	1.27	1.99

3.3.5. Chromatic coordinates and correlated color temperature

Chromaticity, color temperature and purity are fundamental concepts in the field of visual perception, describing respectively the position and hue of a color, the characteristic warmth or coolness of a light source, as well as the purity of the emitted light [85]. The chromatic coordinates (CIE), correlated color temperature (CCT), and color purity (CP) of YPO_4: Sm^{3+} (5 at.%) nanopowder and PNC films were calculated for λ_{ex} = 404 nm at room temperature to assess their potential utility for lighting or display applications. CCT measures the blue or yellow character of light emitted by a bulb and typically falls between 2200 and 6500 K. CIE coordinates were calculated according to CIE 1931 and CIE 1976 (Table. 5) and are shown in Fig. 20(a) and (b), respectively. Detailed calculation procedures for the parameters represented in Table. 5 can be found in references [84-86].

Table. 5 CIE coordinates and color purity calculated for YPO_4: Sm^{3+} (5 at.%) nanopowder and YPO_4: Sm^{3+}/PS, YPO_4: Sm^{3+}/PMMA NC films for λ_{ext} = 404 nm.

Samples	CIE 1931		CIE 1976		Color Purity (%)
	x	y	u'	v'	
Powder 5 at. % Sm^{3+}	0.58538	0.40458	0.35031	0.54475	91.80
NC (5. %) Sm^{3+}/ PMMA	0.57903	0.4056	0.34522	0.54409	86.80
NC (5. %) Sm^{3+} / PS	0.55380	0.39435	0.33439	0.53575	84.70

Based on the data presented in Table 5, all samples have CCT values ranging between 1700 K and 1800 K, which can be described as orange-reddish, similar to that of fire [87]. Compared to the nanopowder sample, the CCT values of NC film samples were close, indicating that YPO_4: Sm^{3+} nano-phosphors retain their original color in the polymer matrix. It was also observed that the CP values of the samples varied within the range of 84.74-91.82 % under λ_{ex} = 404 nm, which is close to red-orange light sources like AlGaInP LED [88]. Ultimately, the study of the chromaticity of composite polymer films loaded with YPO_4:Sm^{3+} nanoparticles demonstrate a beneficial potential for red-orange lighting applications such as display panels, environmentally friendly light sources, microbeam radiotherapy, cathode ray tubes (CRTs), and plasma screens. [87,89].

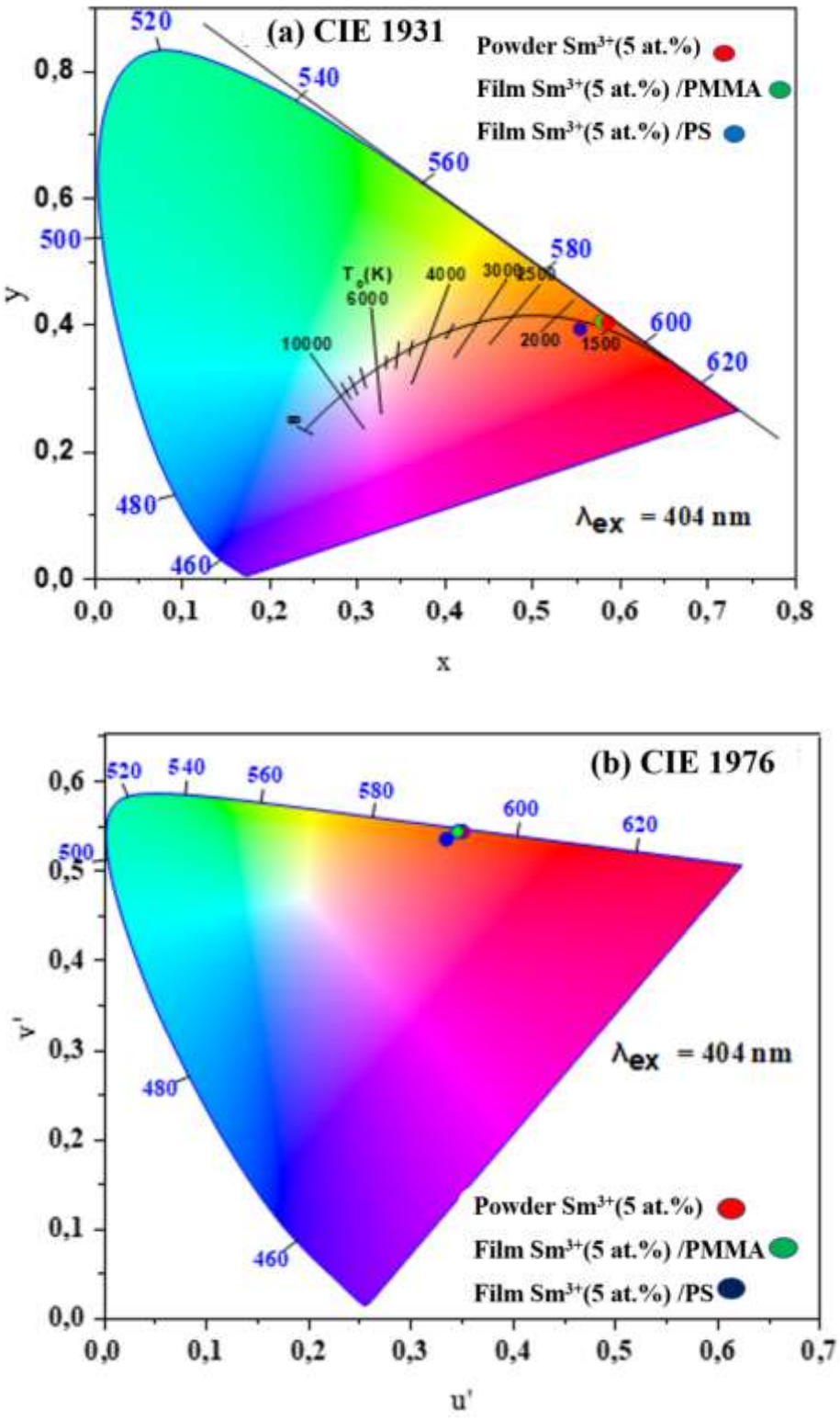

Fig.20 (a) CIE 1931 and (b) CIE 1976 diagrams of YPO_4: (5 at.%) Sm^{3+} nanopowder and YPO_4: Sm^{3+} /PS, YPO_4: Sm^{3+} /PMMA NC films under λ_{ex} = 404 nm.

4. Conclusion

In summary, YPO_4: Sm^{3+}/Polymer flexible luminescent polymer films have been successfully synthesized via the direct mixing method in solution with micrometric thickness. YPO_4: Sm^{3+} (x %. at, x=1, 3, 5, 8, 10) nanophosphors were synthesized using a sol-gel-based experimental protocol. XRD analysis of the nanopowders revealed that all samples crystallized in a pure tetragonal structure, with I_{41}/amd space group, and no other phases were observed. The average crystallite size of the nano-phosphors was estimated to be around 45 nm through Rietveld refinement of the XRD data. The obtained NCs films were subjected to various characterization techniques to examine their structure, morphology, and photoluminescence properties. XRD analysis revealed the characteristics diffraction peaks of YPO_4: Sm^{3+} NPs and polymer matrices. SEM analysis showed the uniform dispersion of luminescent NPs within the surfaces of PMMA and PS polymer films, with more notable dispersion in the PMMA film.. The emission spectra of NPs were recorded under near-UV excitation at 404 nm and are dominated by orange emission (at 601nm) attributed to $^6H_{5/2} \rightarrow {}^4F_{7/2}$ fluorescence of Sm^{3+} ions. The optimal doping concentration of Sm^{3+} was found to be 5 at.%. The photoluminescence spectra of PNC films indicate that the luminescent NPs retain their luminescence behavior while a decrease in luminescence intensity has been observed which is very pronounced in PS based NC film; diminution of 68% (PS NC film) and 32% (PMMA NC film) compared to the proper luminescence intensity of YPO_4: Sm^{3+} NPs. The decay time of luminescent NPs in NC films is shorter than the isolated NPs which due the effective refractive index of NC films effect. The thermal stability of YPO_4: Sm^{3+} (5 at.%) nanophosphor in PMMA was evaluated using TDPL in the 100-400 K range, showing that the nanophosphors retain their luminescent purity at different temperatures, with decreased intensity at high temperatures due to thermal quenching. Color coordinates and correlated color temperature confirmed the red-orange light emission of the prepared phosphors and films. Overall, these results indicate that the obtained luminescent PNC films hold great potential for photonic applications such as orange-LEDs.

Funding Declaration

The authors declare that they have no known competing financial interests or personal relationships that could have appeared to influence the work reported in this paper.

References

[1] HOLONYAK, Nick et BEVACQUA, S. Fo. Coherent (visible) light emission from Ga (As1− xPx) junctions. Applied Physics Letters, 1962, vol. 1, no 4, p. 82-83.

[2] NAKAMURA, Shuji, PEARTON, Stephen, et FASOL, Gerhard. The blue laser diode. The complete story. Measurement Science and Technology, 2001, vol. 12, no 6, p. 755-756.

[3] KOVAC, J., PETERNAI, L., et LENGYEL, O. Advanced light emitting diodes structures for optoelectronic applications. Thin Solid Films, 2003, vol. 433, no 1-2, p. 22-26.

[4] NAKAMURA, Shuji et FASOL, Gerhard. The blue laser diode: GaN based light emitters and lasers. Springer Science & Business Media, 2013.

[5] CHEN, Lei, LIN, Chun-Che, YEH, Chiao-Wen, *et al.* Light converting inorganic phosphors for white light-emitting diodes. Materials, 2010, vol. 3, no 3, p. 2172-2195.

[6] DUDEK, Michał, JUSZA, A., ANDERS, K., *et al.* Luminescent properties of praseodymium doped Y2O3 and LaAlO3 nanocrystallites and polymer composites. Journal of Rare Earths, 2011, vol. 29, no 12, p. 1123-1129.

[7] MUSBAH, Salah S., RADOJEVIĆ, Vesna, BORNA, Nadezda V., et al. PMMA-Y2O3 (Eu3+) nanocomposites: optical and mechanical properties. Journal of the Serbian Chemical Society, 2011, vol. 76, no 8, p. 1153-1161.

[8] PAUL, Donald R. et ROBESON, Lioyd M. Polymer nanotechnology: nanocomposites. Polymer, 2008, vol. 49, no 15, p. 3187-3204.

[9] SHAH, Jasmin, JAN, Muhammad Rasul, et al. Polystyrene degradation studies using Cu supported catalysts. Journal of Analytical and Applied Pyrolysis, 2014, vol. 109, p. 196-204.

[10] HAMROUN, M. S. E., BACHARI, K., GUERBOUS, L., et al. Structural and optical properties of LSO scintillator-polymer composite films. Optik, 2019, vol. 187, p. 111-116.

[11] MACKAY, Michael E., TUTEJA, Anish, DUXBURY, Phillip M., et al. General strategies for nanoparticle dispersion. Science, 2006, vol. 311, no 5768, p. 1740-1743.

[12] SRIRAMOJU, Kishore Kumar et PADMANABHAN, Venkat. Self- Assembly of Bare/Polymer- Grafted Nanoparticle Blends in Homopolymer. Macromolecular Theory and Simulations, 2016, vol. 25, no 6, p. 582-590.

[13] SALADINO, Maria Luisa, ZANOTTO, Antonio, CHILLURA MARTINO, Delia, et al. Ce: YAG nanoparticles embedded in a PMMA matrix: preparation and characterization. Langmuir, 2010, vol. 26, no 16, p. 13442-13449.

[14] NIE, Zhihong, PETUKHOVA, Alla, et KUMACHEVA, Eugenia. Properties and emerging applications of self-assembled structures made from inorganic nanoparticles. Nature nanotechnology, 2010, vol. 5, no 1, p. 15-25.

[15] YOSHIMOTO, Kenji, JAIN, Tushar S., VAN WORKUM, Kevin, et al. Mechanical heterogeneities in model polymer glasses at small length scales. Physical review letters, 2004, vol. 93, no 17, p. 175501.

[16] JIANG, Shan, CHEN, Qian, TRIPATHY, Mukta, et al. Janus particle synthesis and assembly. Advanced materials, 2010, vol. 22, no 10, p. 1060-1071.

[17] KIM, So Youn et ZUKOSKI, Charles F. Role of polymer segment–particle surface interactions in controlling nanoparticle dispersions in concentrated polymer solutions. Langmuir, 2011, vol. 27, no 17, p. 10455-10463.

[18] LEPCIO, Petr, ONDREÁŠ, František, ZÁRYBNICKÁ, Klára, et al. Phase diagram of bare particles in polymer nanocomposites: Uniting solution and melt blending. Polymer, 2021, vol. 230, p. 124033.

[19] KHURSHEED, Sumara, BISWAS, Pankaj, SINGH, Vivek K., et al. Synthesis and optical studies of KCaVO4: Sm3+/PMMA nanocomposites. Vacuum, 2019, vol. 159, p. 414-422.

[20] UPADHYAY, Kanchan, THOMAS, Sabu, VARGHESE, Rini Thresia, et al. Gd2O3: Er3+ embedded PMMA/PC nanocomposites: A luminescent nanocomposite. Polymer Testing, 2021, vol. 93, p. 106911.

[21] DUDEK, Michał, JUSZA, A., ANDERS, K., et al. Luminescent properties of praseodymium doped Y_2O_3 and $LaAlO_3$ nanocrystallites and polymer composites. Journal of Rare Earths, 2011, vol. 29, no 12, p. 1123-1129.

[22] THAKUR, Shashi, DHIMAN, Naresh, SHARMA, Amit, et al. Effect of photonic structure on optical properties of YVO 4: Eu 3+ Phosphor. Journal of Electronic Materials, 2017, vol. 46, p. 2085-2089.

[23] GAO, Guojun, TURSHATOV, Andrey, HOWARD, Ian A., et al. Upconversion fluorescent labels for plastic recycling: a review. Advanced Sustainable Systems, 2017, vol. 1, no 5, p. 1600033.

[24] KUMAR, Ishant et GATHANIA, Arvind K. Photoluminescence and quenching study of the Sm3+-doped LiBaPO4 phosphor. Journal of Materials Science: Materials in Electronics, 2022, vol. 33, no 1, p. 328-341.

[25] KAHOUADJI, Badis, GUERBOUS, Lakhdar, JOVANOVIĆ, Dragana J., et al. Temperature dependence of red emission in $YPO_4:Pr^{3+}$ nanopowders. Journal of Luminescence, 2022, vol. 241, p. 118499.

[26] LAMIRI, Lyes, KAHOUADJI, Badis, ILHAM, Oulkhiari, et al. Structural and photoluminescence investigation of Y_2O_3: Sm^{3+} nanopowders: Organic agent's effect. Vietnam Journal of Chemistry, 2024.,vol.62,no 4,p. 506-516.

[27] SHI, Zhen, SUN, Wenping, WANG, Zhongtao, et al. Samarium and yttrium codoped $BaCeO_3$ proton conductor with improved sinterability and higher electrical conductivity. ACS applied materials & interfaces, 2014, vol. 6, no 7, p. 5175-5182.

[28] SANNAKKI, Basavaraja, et al. Dielectric properties of PMMA and its composites with ZrO2. Physics Procedia, 2013, vol. 49, p. 15-26.

[29] MOHAMMED, M. I., KHAFAGY, R. M., HUSSIEN, Mai SA, et al. Enhancing the structural, optical, electrical, properties and photocatalytic applications of ZnO/PMMA

nanocomposite membranes: Towards multifunctional membranes. Journal of Materials Science: Materials in Electronics, 2021, vol. 33, p. 1-26.

[30] LI, Li, TANG, Xiaohua, JIANG, Zhouqing, *et al.* $NaBaLa_2(PO_4)_3$: a novel host lattice for Sm^{3+}-doped phosphor materials emitting reddish-orange light. Journal of Alloys and Compounds, 2017, vol. 701, p. 515-523.

[31] KAHOUADJI, Badis, MEBARKI, Lamine, BENHARRAT, Lyes, *et al.* Flexible and luminescent polymer nanocomposite films (YPO_4: Pr^{3+}/polystyrene): Investigation of structural, morphological and photoluminescence properties for solid-state lighting applications. Optical Materials, 2023, vol. 143, p. 114251.

[32] BLACK, D. B. et LOVERING, E. G. Estimation of the degree of crystallinity in digoxin by X-ray and infrared methods. Journal of pharmacy and pharmacology, 1977, vol. 29, no 1, p. 684-687.

[33] PARCHUR, Abdul Kareem, PRASAD, Amresh Ishawar, RAI, Shyam Bahadur, *et al*. Observation of intermediate bands in Eu^{3+} doped YPO_4 host: Li^+ ion effect and blue to pink light emitter. AIP Advances, 2012, vol. 2, no 3.

[34] DEVI, Heikham Farida et SINGH, Thiyam David. Comparison on effect of EDTA and citrate mediated on luminescence property of Eu^{3+} doped YPO4 nanoparticles. Perspectives in Science, 2016, vol. 8, p. 267-269.

[35] HERNÁNDEZ, A. Garrido, MURILLO, A. García, ROMO, F. de J. Carrillo, *et al*. Photoluminescence behavior of YPO_4: Tb^{3+} crystallized in monoclinic, hexagonal or tetragonal phase obtained by hydrothermal process. Materials Research Bulletin, 2016, vol. 84, p. 225-231.

[36] DEVI, Heikham Farida et SINGH, Thiyam David. Optical properties of porous Sm^{3+}doped yttrium orthophosphate nanoparticles tailored by co-precipitation route. Optics Communications, 2019, vol. 439, p. 34-37.

[37] MARTÍNEZ ÁVILA, Karen Jaqueline, CARMONA TÉLLEZ, Salvador, BALDERAS AGUILAR, Jesús Uriel, *et al*. Luminescent polymethyl methacrylate composite films activated under infrared radiation, useful for engineering applications. Journal of Photonics for Energy, 2018, vol. 8, no 1, p. 014001-014001.

[38] ENNIS, Courtney P. et KAISER, Ralf I. Mechanistical studies on the electron-induced degradation of polymethylmethacrylate and Kapton. Physical Chemistry Chemical Physics, 2010, vol. 12, no 45, p. 14902-14915.

[39] WURM, Andreas, ISMAIL, Mohamed, KRETZSCHMAR, Bernd, et al. Retarded crystallization in polyamide/layered silicates nanocomposites caused by an immobilized interphase. Macromolecules, 2010, vol. 43, no 3, p. 1480-1487.

[40] TIWARI, Pragya, SRIVASTAVA, A. K., KHATTAK, B. Q., *et al*. Structural modification of poly (methyl methacrylate) due to electron irradiation. Measurement, 2014, vol. 51, p. 1-8.

[41] RAI, V. N., MUKHERJEE, C., et JAIN, Beena. Optical properties (uv-vis and ftir) of gamma irradiated polymethyl methacrylate (pmma). arXiv preprint arXiv:1611.02129, 2016.

[42] RONG, Yu, CHEN, Hong-Zheng, WU, Gang, *et al.* Preparation and characterization of titanium dioxide nanoparticle/polystyrene composites via radical polymerization. Materials Chemistry and Physics, 2005, vol. 91, no 2-3, p. 370-374.

[43] JASSIM, Alwan N., ALWAN, Riyadh M., KADHIM, Quraish A., *et al.* Preparation and characterization of ZnO/polystyrene nanocomposite films using ultrasound irradiation. Nanosci. Nanotechnol, 2016, vol. 6, p. 17-23.

[44] JEEJU, P. P. and JAYALEKSHMI, S. On the interesting optical properties of highly transparent, thermally stable, spin coated polystyrene/zinc oxide nanocomposite films. Journal of Applied Polymer Science, 2011, vol. 120, no 3, p. 1361-1366.

[45] PHETSOMBUN, Thanapong, METANAWIN, Tanapak, et METANAWIN, Siripan. Fabrication of PS-TiO_2 hybrid via mini-emulsion polymerization: Study the effect of crosslink on the photocatalytic properties of the hybrid. Journal of Applied Research on Science and Technology (JARST), 2023, vol. 22, no 3, p. 253757-253757.

[46] YADAV, R. S. et RAI, S. B. Effect of annealing and excitation wavelength on the downconversion photoluminescence of Sm^{3+} doped Y_2O_3 nano-crystalline phosphor. Optics & Laser Technology, 2019, vol. 111, p. 169-175.

[47] DEVI, Heikham Farida et SINGH, Thiyam David. Comparison on effect of EDTA and citrate mediated on luminescence property of Eu^{3+} doped YPO_4 nanoparticles. Perspectives in Science, 2016, vol. 8, p. 267-269.

[48] SEO, Jongchul, JEON, Gwonyoung, JANG, EUi Sung, *et al.* Preparation and properties of poly (propylene carbonate) and nanosized ZnO composite films for packaging applications. Journal of Applied Polymer Science, 2011, vol. 122, no 2, p. 1101-1108.

[49] PRAKASH, Jai, KUMAR, Vinod, ERASMUS, L. J. B., *et al.* Phosphor polymer nanocomposite: ZnO:Tb^{3+} embedded polystyrene nanocomposite thin films for solid-state lighting applications. ACS Applied Nano Materials, 2018, vol. 1, no 2, p. 977-988.

[50] ŠVORČÍK, V., LYUTAKOV, O., et HUTTEL, I. Thickness dependence of refractive index and optical gap of PMMA layers prepared under electrical field. Journal of Materials Science: Materials in Electronics, 2008, vol. 19, p. 363-367.

[51] AZIZ, Shujahadeen B., ABDULLAH, Omed Gh, BRZA, M. A., et al. Effect of carbon nano-dots (CNDs) on structural and optical properties of PMMA polymer composite. Results in Physics, 2019, vol. 15, p. 102776.

[52] WU, Jinxiu, JIA, Hengjun, LI, Mei, *et al.* Influence of pH on nano-phosphor YPO_4: 2% Sm^{3+} and luminescent properties. Applied Physics A, 2020, vol. 126, p. 1-8.

[53] WU, Jinxiu, LI, Mei, JIA, Huiling, *et al.* Morphology formation mechanism and fluorescence properties of nano-phosphor YPO_4:Sm^{3+} excited by near-ultraviolet light. Journal of Alloys and Compounds, 2020, vol. 821, p. 153535.

[54] LEE, Sang Yoon, SAN LIM, Hyung, LEE, Na Eun, *et al.* Biocompatible UV-absorbing polymer nanoparticles prepared by electron irradiation for application in sunscreen. RSC advances, 2020, vol. 10, no 1, p. 356-361.

[55] YADAV, R. S., YADAV, R. V., BAHADUR, A., et al. Role of Li+ on white light emission from Sm^{3+} and Tb^{3+} co-doped Y_2O_3 nano-phosphor. Materials Research Express, 2016, vol. 3, no 3, p. 036201.

[56] KUMAR, Ishant et GATHANIA, Arvind K. Photoluminescence and quenching study of the Sm3+-doped LiBaPO4 phosphor. Journal of Materials Science: Materials in Electronics, 2022, vol. 33, no 1, p. 328-341.

[57] BLASSE, G. P. R. L. Energy transfer in oxidic phosphors. Physics Letters A, 1968, vol. 28, no 6, p. 444-445.

[58] JIN-XIU, Wu, MEI, Li, ZHAO-GANG, Liu, et al. Effects of Doped Concentration and Calcination Temperature on Luminescence Properties of Ca1-xSmxWO4 Phosphors. CHINESE JOURNAL OF INORGANIC CHEMISTRY, 2016, vol. 32, no 1, p. 34-42.

[59] ATUCHIN, Victor V., ALEKSANDROVSKY, A. S., CHIMITOVA, O. D., et al. Electronic structure of β-RbSm (MoO 4) 2 and chemical bonding in molybdates. Dalton Transactions, 2015, vol. 44, no 4, p. 1805-1815.

[60] KAHOUADJI, Badis, GUERBOUS, Lakhdar, JOVANOVIĆ, Dragana J., et al. Photoluminescence properties of nano-sized (Lu_{1-x} Yx) PO_4: Pr^{3+} (x= 10, 20, 30, 40, 50 at.%) phosphor powders. Optical Materials, 2020, vol. 109, p. 110252.

[61] DEXTER, David L. A theory of sensitized luminescence in solids. The Journal of Chemical Physics, 1953, vol. 21, no 5, p. 836-850.

[62] DU, Peng, HUANG, Xiaoyong, et YU, Jae Su. Facile synthesis of bifunctional Eu3+-activated NaBiF4 red-emitting nanoparticles for simultaneous white light-emitting diodes and field emission displays. Chemical Engineering Journal, 2018, vol. 337, p. 91-100.

[63] ANU et RAO, A. S. Synthesis, Structural and Fluorescence Investigations of Novel $Li_2Ba_5W_3O_{15}$: Sm^{3+} Phosphors for Photonic Device Applications. Journal of Fluorescence, 2023, p. 1-13. https://doi.org/10.1007/s10895-023-03449-z

[64] KARA, Hulya, OYLUMLUOGLU, Gorkem, et COBAN, Mustafa Burak. Photoluminescence properties of a new Sm (III) Complex/PMMA electrospun composite fibers. Journal of Cluster Science, 2020, vol. 31, p. 701-708.

[65] RAJAKRISHNA, Kalvala, DHANASEKARAN, A., YUVARAJ, N., et al. Improvement in Plastic Scintillator with Loading of BaFBr: Eu^{2+} Radioluminescence Phosphor. IEEE Transactions on Nuclear Science, 2021, vol. 68, no 6, p. 1286-1295.

[66] NOVAIS, S. M. V., MONTEIRO, T. J., TEIXEIRA, V. C., et al. Hydrothermal synthesis of CdWO4 for scintillator-polymer composite films development. Journal of Luminescence, 2018, vol. 199, p. 225-231.

[67] MASTOUR, Nouha et BOUCHRIHA, Habib. Effect of CdSe nanoparticles on the fluorescence spectra of conjugate polymer P3HT: An experimental and theoretical study. Physics Letters A, 2016, vol. 380, no 45, p. 3866-3869.

[68] DENDEBERA, M., ZHYSHKOVYCH, A., MALYI, T. S., et al. Polystyrene composites with loaded laf 3 nanoparticles for registration of ionizing radiation. Journal of Physical Studies, 2020, vol. 24, no 4, p. 1-5.

[69] V. Țucureanu , A. Matei, A. Avram , The effect of the polymeric matrix on the emission properties of YAG-based phosphors, J. Alloys Compd., 2020, vol. 844, 156136.

[70] YAMAMOTO, Hajime. White LED phosphors: the next step. Optical Components and Materials VII, 2010, vol. 7598, p. 73-82.

[71] RAKOV, Nikifor, VIEIRA, Simone A., SILVA, Queli PS, et al. Facile fabrication of Eu^{3+}-doped lanthanum oxyfluoride powders by combustion processes and temperature analysis of its fluorescence for thermal sensor application. Sensors and Actuators B: Chemical, 2015, vol. 209, p. 407-412.

[72] DORENBOS, Pieter. Thermal quenching of lanthanide luminescence via charge transfer states in inorganic materials. Journal of Materials Chemistry C, 2023, vol. 11, no 24, p. 8129-8145.

[73] SON, Nguyen Manh, TIEN, Do Thanh, LIEN, Nguyen Thi Quynh, et al. Luminescence and Thermal-Quenching Properties of Red-Emitting $Ca_2Al_2SiO_7$: Sm^{3+} Phosphors. Journal of Electronic Materials, 2020, vol. 49, p. 3701-3707.

[74] ZHAO, Lei, FAN, Feiyue, CHEN, Xiao, et al. Luminescence and thermal-quenching properties of silicate-based red-emitting $K_4CaSi_3O_9$: Eu^{3+} phosphor. Journal of Materials Science: Materials in Electronics, 2018, vol. 29, no 7, p. 5975-5981.

[75] GUO, Ning, HUANG, Yeju, YANG, Mei, et al. A tunable single-component warm white-light $Sr_3Y(PO_4)_3$: Eu^{2+}, Mn^{2+} phosphor for white-light emitting diodes. Physical Chemistry Chemical Physics, 2011, vol. 13, no 33, p. 15077-15082.

[76] N. Pradal, D. Boyer, G. Chadeyron, S. Therias, A. Chapel, C. V. Santillid , R. Mahiou, Investigations on PVP/Y_3BO_6:Eu^{3+}, a red luminescent composite for lighting devices based on near UV LEDs, J. Mater. Chem. C., 2014, vol. 2, 6301–6311.

[77] A.Juszaa, L. Lipińska, M. Baran, A. Olszyna, A. Jastrzębska, M.Gild, P. Mergo, R. Piramidowicz, Praseodymium doped nanocrystals and nanocomposites for application in white light sources, Opt Mate. 95 (2019) 109247.

[78] MELTZER, R. S, FEOFILOV, S. P, TISSUE, B, et al. Dependence of fluorescence lifetimes of Y_2O_3: Eu $^{3+}$ nanoparticles on the surrounding medium. Physical Review B, 1999, vol. 60, no 20, p. R14012.

[79] KRSMANOVIĆ, Radenka M., ANTIĆ, Željka, NIKOLIĆ, Marko G., et al. Preparation of Y_2O_3: Eu^{3+} nanopowders via polymer complex solution method and luminescence properties of the sintered ceramics. Ceramics International, 2011, vol. 37, no 2, p. 525-531.

[80] RAJAKRISHNA, Kalvala, DHANASEKARAN, A., YUVARAJ, N., et al. Improvement in Plastic Scintillator with Loading of BaFBr: Eu^{2+} Radioluminescence Phosphor. IEEE Transactions on Nuclear Science, 2021, vol. 68, no 6, p. 1286-1295.

[81] CAVALLI, Enrico. Optical spectra and excited state dynamics of Sm^{3+}-doped YVO_4 and YPO_4 crystals. Journal of Luminescence, 2017, vol. 183, p. 173-177.

[82] SALADINO, Maria Luisa, ZANOTTO, Antonio, CHILLURA MARTINO, Delia, et al. Ce: YAG nanoparticles embedded in a PMMA matrix: preparation and characterization. Langmuir, 2010, vol. 26, no 16, p. 13442-13449.

[83] NINGTHOUJAM, R. S., SHARMA, Anusha, SHARMA, K. S., et al. Roles of solvent, annealing and Bi^{3+} co-doping on the crystal structure and luminescence properties of YPO_4 : Eu^{3+} nanoparticles. RSC Advances, 2015, vol. 5, no 83, p. 68234-68242.

[84] DURMUS, D. Correlated color temperature: Use and limitations. Lighting Research & Technology, 2022, vol. 54, no 4, p. 363-375.

[85] Sanjeeb Limbu, Laishram Robindro Singh, Exploring luminescent color tunability and efficient energy transfer mechanism of a single-phased hexagonal nanophosphor for white light emitting diodes (WLEDs) application, Journal of Alloys and Compounds, 2024, vol.970,p.172580.

[86] E. H. H. Ha sabeldaim**,** H. C. Swart, R. E. Kroon, Luminescence and stability of Tb doped CaF_2 nanoparticles. RSC Adv, 2023, vol. 13,p. 5353-5366.

[87] SAGAR, S. Vidya, BABU, S., et RAO, K. Venkata. Emission spectroscopy of Sm^{3+} ion-activated zinc phosphate glass for reddish-orange lighting applications. Journal of Materials Science: Materials in Electronics, 2023, vol. 34, no 33, p. 2216.

[88] E.F. Schubert, Light Emitting Diodes, 2nd ed., Cambridge University Press, New York, 2018.

[89] RAJAGUKGUK, Juniastel, SITUMORANG, Rappel, NASUTION, Budiman, et al. Synthesis and Structural Properties of Sm^{3+} doped Sodium Lithium zinc Lead Borate Glasses. In : Journal of Physics: Conference Series. IOP Publishing, 2021. p. 012112.